

1 **TITLE**

2 **Mapping peat thickness and carbon stocks of the central Congo Basin using**
3 **field data**

4

5 **AUTHOR LIST**

6 Bart Crezee¹, Greta C. Dargie¹, Corneille E.N. Ewango^{2,3}, Edward T.A. Mitchard⁴,
7 Ovide Emba B.⁵, Joseph Kanyama T.², Pierre Bola⁵, Jean-Bosco N. Ndjango³,
8 Nicholas T. Girkin⁶, Yannick E. Bocko⁷, Suspense A. Ifo⁸, Wannes Hubau^{9,10}, Dirk
9 Seidensticker¹¹, Rodrigue Batumike¹², Gérard Imani¹³, Aida Cuní-Sanchez^{14,15},
10 Christopher A. Kiahtipes¹⁶, Judicaël Lebamba^{17,18}, Hans-Peter Wotzka¹⁷, Hollie
11 Bean¹⁹, Timothy R. Baker¹, Andy J. Baird¹, Arnoud Boom¹⁹, Paul J. Morris¹, Susan E.
12 Page¹⁹, Ian T. Lawson²⁰, Simon L. Lewis^{1,21}

13

14 **AFFILIATIONS**

15 ¹ *School of Geography, University of Leeds, Leeds, LS2 9JT, UK*

16 ² *Faculté de Gestion des Ressources Naturelles Renouvelables, Université de*
17 *Kisangani, Kisangani, Democratic Republic of the Congo*

18 ³ *Faculté des Sciences, Université de Kisangani, Kisangani, Democratic Republic of*
19 *the Congo*

20 ⁴ *School of GeoSciences, University of Edinburgh, Edinburgh, EH9 3FF, UK*

21 ⁵ *Institut Supérieur Pédagogique de Mbandaka, Mbandaka, Democratic Republic of*
22 *the Congo*

23 ⁶ *School of Water, Energy and Environment, Cranfield University, Cranfield, MK43*
24 *0AL, UK*

25 ⁷ *Laboratoire de Botanique et Ecologie, Faculté des Sciences et Techniques,*
26 *Université Marien Ngouabi, Brazzaville, Republic of the Congo*

27 ⁸ *École Normale Supérieure, Département des Sciences et Vie de la Terre,*
28 *Laboratoire de Géomatique et d'Ecologie Tropicale Appliquée, Université Marien*
29 *Ngouabi, Brazzaville, Republic of the Congo*

30 ⁹ *Department of Environment, Laboratory of Wood Technology, Ghent University,*
31 *9000 Ghent, Belgium*

32 ¹⁰ *Service of Wood Biology, Royal Museum for Central Africa, 3080 Tervuren, Belgium*

33 ¹¹ *Department of Archaeology, Ghent University, 9000 Ghent, Belgium*

34 ¹² *Département des Sciences de l'Environnement, Université du Cinquenaire de*
35 *Lwiro, Kabare, Sud-Kivu, Democratic Republic of the Congo*

36 ¹³ *Département de Biologie, Université Officielle de Bukavu, Bukavu, Democratic*
37 *Republic of the Congo*

38 ¹⁴ *Department of Environment and Geography, University of York, York, YO10 5NG,*
39 *UK*

40 ¹⁵ *Department of International Environmental and Development Studies (NORAGRIC),*
41 *Norwegian University of Life Sciences, 1433 Ås, Norway*

42 ¹⁶ *Institute for the Advanced Study of Culture and the Environment, University of South*
43 *Florida, Tampa, FL 33620, USA*

44 ¹⁷ *Department of Prehistoric Archaeology, University of Cologne, 50931 Köln,*
45 *Germany*

46 ¹⁸ *Département de Biologie, Université des Sciences et Techniques de Masuku, BP*
47 *943, Franceville, Gabon*

48 ¹⁹ *School of Geography, Geology & the Environment, University of Leicester,*
49 *Leicester, LE1 7RH, UK*

50 ²⁰ *School of Geography and Sustainable Development, University of St Andrews, St*
51 *Andrews, KY16 9AL, UK*

52 ²¹ *Department of Geography, University College London, London, WC1E 6BT, UK*

53

54

55 **CORRESPONDING AUTHOR**

56 Correspondence and requests for materials should be addressed to B.C.
57 (crezeebart@gmail.com).

58

59 **ABSTRACT**

60 The world's largest tropical peatland complex is found in the central Congo Basin.
61 However, there is a lack of *in situ* measurements needed to understand the peat's
62 distribution and the amount of carbon stored in it. So far, peat in this region has only
63 been sampled in largely rain-fed interfluvial basins in the north of the Republic of the
64 Congo. Here we present the first extensive field surveys of peat in the Democratic
65 Republic of the Congo, which covers two-thirds of the estimated peatland area,
66 including from previously undocumented river-influenced settings. We use field data
67 from both countries to compute the first spatial models of peat thickness (mean $1.7 \pm$
68 0.9 m; maximum 5.6 m) and peat carbon density (mean $1,712 \pm 634$ Mg C ha⁻¹;
69 maximum 3,970 Mg C ha⁻¹) for the basin. We show that the peatland complex covers
70 167,600 km², 15% more than previously estimated, and that 29.0 Pg C is stored
71 belowground in peat across the region (95% confidence interval, 26.3-32.2 Pg C). Our
72 measurement-based constraints give high confidence of globally significant peat
73 carbon stocks in the central Congo Basin, totalling approximately one-third of the
74 world's tropical peat carbon. Only 8% of this peat carbon lies within nationally
75 protected areas, suggesting its vulnerability to future land-use change.

76 **MAIN TEXT**

77 Peatlands cover just 3% of Earth's land surface¹, yet store an estimated 600 Pg of
78 carbon (C)^{2,3}, approximately one-third of Earth's soil carbon⁴. While most peatlands
79 are located in the temperate and boreal zones¹, recent research is revealing the
80 existence of tropical peatlands with high carbon densities^{1,2,5,6}. Tropical peatlands are
81 vulnerable to drainage and drying, with subsequent fires resulting in large carbon
82 emissions from degraded peatlands, particularly in Southeast Asia^{3,6-8}.

83

84 In the central depression of the Congo basin (the 'Cuvette Centrale') the only field-
85 verified peatland map to date reported that peat underlies 145,500 km² of swamp
86 forests, making this the world's largest tropical peatland complex⁹. The field data used
87 in this estimate are from northern Republic of the Congo (ROC), yet two-thirds of the
88 central Congo Basin peatlands are predicted to be found in neighbouring Democratic
89 Republic of the Congo (DRC)⁹, sometimes hundreds of kilometres from existing field
90 data (Figure 1a). Similarly, peat carbon stocks are estimated to be 30.6 Pg C, but the
91 lower confidence interval is just 6 Pg C (ref. ⁹). Thus, it is unclear if the central Congo
92 peatlands are truly as extensive or deep as suggested, and it is unclear whether they
93 store globally significant quantities of carbon.

94

95 Uncertainties are further compounded by a limited understanding of the processes
96 that determine peat formation in central Congo, particularly hydrology^{9,10}. Peat has
97 only been systematically documented in interfluvial basins in ROC^{9,11}, where an
98 absence of annual flood waves⁹, modest domes¹², and remotely-sensed water-table
99 depths¹³ all suggest peatlands are largely rain-fed and receive little river water input.
100 However, peat is also predicted in other hydro-geomorphological settings⁹, including

101 what appear to be river-influenced regions close to the Congo River mainstem and
102 dendritic-patterned valley-floors along some of its left-bank tributaries⁹ (Figure 1a).
103 These areas of swamp forest are likely seasonally inundated¹⁴ to depths up to 1.5 m
104 during the main wet season¹⁵, suggesting seasonal river flooding and/or upland runoff
105 as key sources of water. Whether peat accumulates under these river-influenced
106 conditions is currently unknown.

107

108 Here, we present the first *in situ* data on peat presence, thickness, and carbon density
109 (mass per unit area) from the central Congo Basin in DRC. We specifically investigated
110 the river-influenced swamp forests along the Congo River and its Ruki, Busira and
111 Ikelemba tributaries that contrast with previous data collection from interfluvial basins⁹
112 (Figure 1a). Every 250 m along 18 transects, we recorded vegetation characteristics,
113 peat presence and thickness. We targeted a first group of ten transects in locations
114 highly likely to contain peat, to help test hypotheses (detailed in Supplementary Table
115 1) about the role of vegetation, surface wetness, nutrient status, and topography in
116 peat accumulation. To improve mapping capabilities, we sampled a second group of
117 eight transects specifically to test preliminary maps that gave conflicting results or
118 suspected false predictions of peat presence (detailed in Supplementary Table 1). We
119 combine these new field measurements from DRC with previous transect records in
120 ROC using the same protocols⁹ and other ground-truth data (Supplementary Table 2)
121 to produce (i) a second-generation map of peatland extent, (ii) a first-generation map
122 of peat thickness, and (iii) a first-generation map of belowground peat carbon density
123 for the central Congo Basin. These maps enable us to compute the first well-
124 constrained estimate of total belowground peat carbon stocks in the world's largest
125 tropical peatland complex.

126

127 ***Mapping peatland extent***

128 We found peat along all ten hypothesis-testing transects in DRC that were predicted
129 to be peatlands⁹. Our new field data shows that extensive carbon-rich peatlands are
130 present in the forested wetlands of the DRC's Cuvette Centrale, including in
131 geomorphologically distinct river-influenced regions predicted as peatlands by Dargie
132 et al.⁹.

133

134 The best-performing algorithm (Maximum Likelihood classifier, based on its ability to
135 most accurately predict in regions with no training data; see Methods) was run 1,000
136 times on nine remotely-sensed datasets, using a random two-thirds of 1,736 ground-
137 truth datapoints each time (Extended Data Figure 1), giving a median total peatland
138 area for the central Congo Basin of 167,600 km² (95% CI, 159,400-175,100 km²). This
139 is 15% higher than the previous estimate⁹. We found that 90% of all pixels that are
140 predicted as peat in the median map result were predicted as peat in at least 950 out
141 of 1,000 runs (i.e., with $\geq 95\%$ probability, either as hardwood- or palm-dominated peat
142 swamp forest; Figure 1b), showing that peat predictions are consistent across model
143 runs and thus are robust. Overall model performance, using the Matthews correlation
144 coefficient, is 78.0% (95% CI, 74.2-81.6%).

145

146 Comparing our field results with the original first-generation map⁹ shows that of the
147 382 locations assessed across DRC, 77.7% were correctly classified as either being
148 peat swamp or not by the first-generation map⁹. Comparing our new map with the first-
149 generation map⁹ shows large areas of agreement (white in Figure 1c). However, we
150 predict areas of peat which were previously not mapped⁹, particularly around Lake

151 Mai-Ndombe and the Ngiri and upper Congo/Lulonga Rivers in DRC (red in Figure
152 1c). In addition, small areas of previously predicted peat deposits⁹ are no longer
153 predicted by our new model, particularly along the Sangha and Likouala-Mossaka
154 Rivers in ROC (blue in Figure 1c). These areas of difference are likely areas of high
155 uncertainty and should therefore be priorities for future fieldwork.

156

157 More formally, we compare our new second-generation map with the original map⁹
158 using balanced accuracy (BA), which is similar to Matthews correlation coefficient but
159 better suited for comparison across different datasets¹⁶. For our new map, median BA
160 is 91.9% (95% CI, 90.2-93.6%), compared with 89.8% (86.0-93.4%) for the first-
161 generation map⁹. The substantially smaller BA interval indicates improved confidence
162 in our new peatland map, despite only a small increase in median BA. This is likely
163 due to the effect of our larger sample size being partly offset by an increase in its
164 spatial extent and ecological diversity, particularly data from the Congo River region,
165 where all algorithms that we tested are underperforming (Supplementary Table 3).
166 Overall, our *in situ* data from DRC, including from river-influenced settings that are
167 being reported for the first time, confirm the central Congo Basin peatlands as the
168 world's largest tropical peatland complex, and that DRC and ROC are the second and
169 third most important countries in the tropics for peatland area after Indonesia⁵,
170 respectively (Extended Data Figure 2).

171

172 ***Mapping peat thickness and carbon density***

173 We measured peat thickness at 238 locations in DRC (including 59 laboratory-verified
174 measurements; Extended Data Figure 3), finding a mean (\pm s.d.) thickness of 2.4 (\pm
175 1.6) m and a maximum of 6.4 m. This shows that river-influenced peatlands can attain

176 similar peat thickness as rain-fed interfluvial basins reported in ROC⁹ (Table 1). There
177 is no uniform increase in peat thickness with distance from the peatland margin
178 (Extended Data Figure 4), with linear regression being only a modest fit ($R^2 = 41.0\%$;
179 RMSE = 1.21 m). Thus, we developed a Random Forest (RF) regression to estimate
180 peat thickness, using 463 thickness measurements across both countries. Our final
181 RF model includes four predictors after variable selection (see Methods): distance
182 from the peatland margin, precipitation seasonality, climatic water balance
183 (precipitation minus potential evapotranspiration), and distance from the nearest
184 drainage point ($R^2 = 93.4\%$; RMSE = 0.42 m). The RF model outperforms multiple
185 linear regression with interactions using the same four variables (adj- $R^2 = 73.6\%$,
186 RMSE = 0.80 m; Extended Data Figure 5).

187

188 Spatially, we predict thick peat deposits in the centres of the largest interfluvial basins
189 (far from peatland margins), and in smaller, river-influenced valley-floor peatlands
190 along the Ruki/Busira Rivers (Figure 2a). The river valley's thick deposits are most
191 likely driven by greater climatic water balance and lower precipitation seasonality in
192 the eastern part of the Cuvette Centrale region (Extended Data Figure 6), plus
193 potentially greater water inputs from nearby higher ground, which offsets the shorter
194 distances from peatland margins. Our modelled results are consistent with our field
195 data, as the two deepest peat cores are from the interfluvial Centre transect in ROC
196 (5.9 m), and the river-influenced Bondamba transect on the Busira River in DRC (6.4
197 m). Overall, mean (\pm s.d.) modelled peat thickness (1.7 ± 0.9 m) is lower than our field
198 measurements (2.4 ± 1.5 m; Table 1), as expected given our linear transects, which
199 oversample deeper peat at the centre relative to the periphery in approximately ovoid
200 peatlands. Areas of high uncertainty in peat thickness occur where distance from the

201 margin is uncertain (Figure 2b). Our results contrast strongly with an “expert system
202 approach” that assigned peat thickness values based on hydrological terrain relief
203 alone and estimated a thickness of 6.5 ± 3.5 m for the central Congo Basin
204 peatlands¹⁷, compared to our field-derived estimate of 1.7 ± 0.9 m (Figure 2a).

205

206 After distance from the margin, precipitation seasonality and climatic water balance
207 are the most important predictors of peat thickness in the RF model, reflecting the
208 relative importance of rainfall inputs in peat accumulation in central Congo. This
209 appears to differ from smaller-scale assessments in temperate¹⁸ or other tropical
210 peatlands¹⁹, where surface topography (elevation and slope) are primary predictors of
211 peat thickness. However, this is potentially merely an artefact of the spatial scale of
212 the studies, as climate only varies over large scales. Alternatively, the relatively low
213 rainfall in the central Congo Basin (~ 1700 mm yr⁻¹), compared to other tropical
214 peatland regions (e.g., $\sim 2,500$ - $3,000$ mm yr⁻¹ in Northwest Amazonia and Southeast
215 Asia)^{9,20}, may mean that peat thickness is more strongly related to climate in central
216 Congo, as it implies greater exposure to (seasonal) drought conditions that may cross
217 thresholds that negatively impact peat accumulation rates.

218

219 Peat bulk density measured across the central Congo Basin is 0.17 ± 0.06 g cm⁻³
220 (mean \pm s.d.; n = 80 cores), and mean carbon concentration is 55.7 ± 3.2 % (n = 80;
221 $56.6 [\pm 4.5]$ % for the 22 well-sampled cores). While peat bulk density is significantly
222 lower in largely river-influenced sites than in rain-fed interfluvial basins ($P < 0.01$), no
223 significant difference between these peatland types is found for either peat carbon
224 concentration or carbon density (mass per unit area; Table 1).

225

226 We used the peat thickness, bulk density, and carbon concentration measurements to
227 construct a linear peat thickness-carbon density regression (Extended Data Figure 7).
228 We applied this regression model to our peat thickness map to spatially model carbon
229 stocks per unit area (Figure 3a). Modelled belowground peat carbon density for the
230 central Congo Basin is $1,712 \pm 634 \text{ Mg C ha}^{-1}$, similar to the field-measured mean of
231 $1,741 \pm 1,186 \text{ Mg C ha}^{-1}$ (mean \pm s.d., $n = 80$; Table 1). This carbon density is
232 approximately nine times the mean carbon stored in aboveground live tree biomass of
233 African tropical moist forests ($\sim 198 \text{ Mg C ha}^{-1}$)²¹. Compared with recently mapped
234 peatlands in the lowland Peruvian Amazon (mean 867 Mg C ha^{-1})²², the central Congo
235 peatlands store almost twice as much carbon per hectare. Spatial patterns of peat
236 carbon density (Figure 3a) and uncertainty (Figure 3b) follow similar patterns as peat
237 thickness (Figures 2a and 2b).

238

239 ***Estimating basin-wide peat carbon stocks***

240 Median estimated total peat carbon stock in the central Congo Basin is 29.0 Pg (95%
241 CI, 26.3-32.2; Extended Data Figure 8a), based on bootstrapping the area estimate
242 and peat thickness-carbon density regression. This is similar to the median 30.6 Pg C
243 reported by Dargie et al.⁹, but their lower 95% confidence interval was 6.3 Pg, which
244 our study increases to 26.3 Pg. This constraint on the carbon stock estimate is possible
245 because our larger field-based dataset allows a spatial modelling approach, so that
246 we can sum carbon density across all peat pixels. Therefore, the possibility of low
247 values of carbon storage in the central Congo peatlands can now confidently be
248 discarded.

249

250 Our new results show that the central Congo Basin peatlands are a globally important
251 carbon stock, harbouring approximately one-third of all the carbon stored in the world's
252 tropical peatlands^{5,9}. About two-thirds of this peat carbon is in DRC (19.6 Pg C; 95%
253 CI, 17.9-21.9), and one-third in ROC (9.3 Pg C; 95% CI, 8.4-10.2; Extended Data
254 Figure 2), which is equivalent to approximately 82% and 238% of each country's
255 aboveground forest carbon stock, respectively²³. The high peat carbon stocks are
256 found across several administrative regions in both countries, with the largest stocks
257 in DRC's Équateur province (Extended Data Figure 2). Sensitivity analysis shows that
258 uncertainty in total peat carbon stock is now mostly driven by uncertainty in peatland
259 area (Extended Data Figure 8b).

260

261 Because the central Congo peatlands are relatively undisturbed^{24,25}, our new maps of
262 peatland extent, thickness and carbon density form a baseline description for the
263 decade 2000-2010, given the remotely-sensed data used. Today, the peatlands of the
264 central Congo Basin are threatened by hydrocarbon exploration, logging, palm oil
265 plantations, hydroelectric dams and climate change^{24,26}. While the peatlands are
266 largely within a UN Ramsar Convention transboundary wetland designation, we
267 estimate that only 2.4 Pg C in peat, just 8% of total stocks, currently lies within formal
268 national-level protected areas (Extended Data Figures 9 and 10). Meanwhile, logging,
269 mining, or palm oil concessions together overlie 7.4 Pg C in peat, or 26% of total stocks
270 (Extended Data Figures 9 and 10), while hydrocarbon concessions cover almost the
271 entire peatland complex^{24,26}.

272

273 Keeping the central Congo Basin peatlands wet is vital to prevent peat carbon being
274 released to the atmosphere. The identification of extensive river-influenced peatlands

275 suggests that there is more than one geomorphological setting where peat is found in
276 the central Congo Basin. Further work is required to understand both the sources and
277 flows of water in these river-influenced peatlands, specifically the relative contributions
278 of water from precipitation, riverbank overflow, and run-off from higher ground to peat
279 formation and maintenance. Given the current areas of formal protection of peatlands
280 are largely centred around interfluvial basins, we suggest that additional protective
281 measures will be needed to safeguard the newly identified river-influenced peatlands
282 of the central Congo Basin. Keeping the central Congo peatlands free from
283 disturbance would also help protect the rich biodiversity, including forest elephants,
284 lowland gorillas, chimpanzees and bonobos^{24,27,28}, that form part of this globally
285 important, but threatened ecosystem.

286 **METHODS**

287

288 ***Field data collection***

289 Fieldwork was conducted in DRC between January 2018 and March 2020. Ten
290 transects (4-11 km long) were installed, identical to Dargie et al.'s approach⁹, in
291 locations that were highly likely to be peatland. These were selected to help test
292 hypotheses about the role of vegetation, surface wetness, nutrient status, and
293 topography in peat accumulation (Figure 1a; Supplementary Table 1). A further eight
294 transects (0.5-3 km long) were installed to assess our peat mapping capabilities
295 (Figure 1a; Supplementary Table 1).

296

297 Every 250 m along each transect, landcover was classified as one of six classes:
298 water, savanna, *terra firme* forest, non-peat forming seasonally inundated forest,
299 hardwood-dominated peat swamp forests, or palm-dominated peat swamp forests.
300 Peat swamp forest was classified as palm-dominated when > 50% of the canopy,
301 estimated by eye, were palms (commonly *Raphia laurentii* or *Raphia sese*). In addition,
302 several ground-truth points were collected at locations in the vicinity of each transect
303 from the clearly identifiable landcover classes water, savanna, or *terra firme* forest.

304

305 Peat presence/absence was recorded every 250 m along all transects, and peat
306 thickness (if present) was measured by inserting metal poles into the ground until the
307 poles were prevented from going any further by the underlying mineral layer, identical
308 to Dargie et al.'s pole-method⁹. Additionally, a core of the full peat profile was extracted
309 every kilometre along the ten hypothesis-testing transects, if peat was present, with a

310 Russian-type corer (52-mm stainless steel Eijkelkamp model); these 63 cores were
311 sealed in plastic for laboratory analysis.

312

313 ***Peat thickness laboratory measurements***

314 Peat was defined as having an organic matter (OM) content of $\geq 65\%$ and a thickness
315 of ≥ 0.3 m (*sensu* Dargie et al.⁹). Therefore, down-core OM content of all 63 cores was
316 analysed to measure peat thickness. The organic matter content of each 0.1-m thick
317 peat sample was estimated via Loss-On-Ignition (LOI), whereby samples were heated
318 at 550°C for 4h. The mass fraction lost after heating was used as an estimate of total
319 OM content (% of mass). Peat thickness was defined as the deepest 0.1-m with OM
320 $\geq 65\%$, after which there is a transition to mineral soil. Samples below this depth were
321 excluded from further analysis. Rare mineral intrusions into the peat layer above this
322 depth, where OM $< 65\%$ for a sample within the peat column, were retained for further
323 analysis. In total, 59 out of 63 collected cores had LOI-verified peat thickness ≥ 0.3 m.

324

325 The pole-method used to estimate peat thickness in the field was calibrated against
326 LOI-verified measurements, by fitting a linear regression model between all LOI-
327 verified and pole-method peat thickness measurements sampled at the same location
328 (93 sites across ROC and DRC, including 37 from ref. ⁹). Three measurements from
329 DRC with a Cook's distance $> 4x$ the mean Cook's distance were excluded as
330 influential outliers. Mean pole-method offset was significantly higher along the DRC
331 transects (0.94 m) than along those in ROC (0.48 m; $P < 0.001$), due to the presence
332 of softer alluvium substrate in river-influenced sites in DRC. We therefore added this
333 grouping as a categorical variable to the regression. The resulting model ($\text{adj-R}^2 =$
334 0.95, $P < 0.001$; Extended Data Figure 3) was used to correct all pole-method

335 measurements in each group for which no LOI-verified thickness was available:
336 corrected peat thickness = $-0.1760 + 0.8626 \times (\text{pole-method thickness}) - 0.3284 \times$
337 (country), with country dummy coded as: ROC (0) and DRC (1).

338

339 ***Carbon density estimates***

340 To calculate carbon density (mass per unit area), estimates of carbon storage in each
341 0.1-m thick peat sample (thickness \times bulk density \times carbon concentration) were
342 summed to provide an estimate of total carbon density per core (in Mg C ha⁻¹),
343 identical to Dargie et al.⁹. We estimated carbon density for 80 peat cores (OM \geq 65%,
344 thickness \geq 0.3 m), located every other kilometre along 18 transects, including 37
345 cores from the ten transects used for hypothesis testing in DRC, and 43 cores from
346 transects in ROC⁹.

347

348 Peat thickness of the 80 cores was obtained by laboratory LOI. To estimate peat bulk
349 density, every other 0.1-m down-core, samples of a known peat volume were weighed
350 after being dried for 24h at 105°C (n = 906). Bulk density (in g cm⁻³) was then
351 calculated by dividing the dry sample mass (in g) by the volume of the sample taken
352 from the peat corer dimensions (in cm³). Within each core, linear interpolation was
353 used to estimate bulk density for the alternate 0.1m-thick samples of the core that were
354 not measured.

355

356 For total carbon concentration (%), only the deepest core per transect, plus additional
357 deep cores from the Lokolama transect (1) in DRC and Ekolongouma transect (3) in
358 ROC (22 in total, 11 from DRC and 11 from ROC⁹) were sampled down-core. Every
359 other 0.1-m thick sample was measured using an elemental analyser (Elementar Vario

360 MICRO Cube with thermal conductivity detection for all cores, except those from
361 Boboka, Lobaka and Ipombo transects, which were analysed using Sercon ANCA
362 GSL with isotope-ratio mass spectrometer detection, due to COVID-19 disruption). All
363 samples (n = 422) were pre-dried for 48h at 40°C and ground to < 100 µm using a
364 MM301 mixer mill. Again, linear interpolation was used within each core for the
365 alternate samples that were not measured.

366

367 The remaining 58 cores had less-intensive carbon concentration sampling. We
368 therefore interpolated the carbon concentration for each 0.1-m thick sample, because
369 well-sampled cores show a consistent pattern with depth: an increase to a depth of
370 about 0.5 m, followed by a long, very weak decline, and finally a strong decline over
371 the deepest approximately 0.5 m of the core⁹. We used segmented regression on the
372 22 well-sampled cores (*segmented* package in R, version 1.3-1) to parameterize the
373 three sections of the core, using the means of these relationships to interpolate carbon
374 concentrations for the remaining 58 cores, following Dargie et al.⁹.

375

376 To estimate carbon density from modelled peat thickness across the basin, we
377 developed a regression model between peat thickness and per-unit-area carbon
378 density using the 80 sampled cores. We compared linear regressions for normal,
379 logarithmic-, and square root-transformed peat thickness, selecting the model with
380 lowest AICc and highest R². A linear model with square root-transformed peat
381 thickness was found to provide the best fit (R² = 0.86; P < 0.001; Extended Data Figure
382 7). Bootstrapping was applied (*boot* package in R, version 1.3-25) to assess
383 uncertainty around the regression.

384

385 ***Modelling peatland extent***

386 Satellites cannot detect peat directly. We therefore mapped vegetation and used field-
387 based associations between peat and vegetation to infer peat presence^{9,29}. Five
388 landcover classes were used for the purpose of peatland mapping: water, savanna,
389 palm-dominated peat swamp forest, hardwood-dominated peat swamp forest, and
390 non-peat forming forest. In this classification, field recordings of non-peat forming
391 seasonally inundated forest (< 30 cm thickness of $\geq 65\%$ OM) were grouped together
392 with field recordings of *terra firme* forest, which also does not form peat, to form the
393 non-peat forming forest class. Our field recordings of hardwood- or palm-dominated
394 peat swamp forest, by definition, consist of all forest sites that form peat, including any
395 seasonally inundated forest that forms peat (≥ 30 cm of $\geq 65\%$ OM).

396

397 A total of 1,736 ground-truth datapoints was used: 172 in water, 476 in savanna, 632
398 in non-peat forming forest (97 non-peat forming seasonally inundated forest, and 535
399 *terra firme* forest), 188 in palm-dominated peat swamp forest, and 268 in hardwood-
400 dominated peat swamp forest (Extended Data Figure 1). This data comes from eight
401 sources (Supplementary Table 2). First, ground-truth locations collected for this study
402 using a GPS (Garmin GPSMAP 64s) at all transect sites in DRC for which a landcover
403 class was determined (382 points). Second, published ground-truth data from nine
404 transects in ROC (292 points)⁹. Third, 299 GPS locations of known savanna and *terra*
405 *firme* forest landcover classes from archaeological research databases across the
406 basin^{30,31}. Fourth, 191 GPS locations from permanent long-term forest inventory plots
407 of the African Tropical Rainforest Observation Network (AfriTRON), mostly from *terra*
408 *firme* forest³², retrieved from the ForestPlots database^{33,34}. Fifth, 229 GPS datapoints
409 from *terra firme* forest or savanna locations in and around Lomami National Park (*pers.*

410 *comm.*, R.B., G.I. and A. C-S.). Sixth, 24 published savanna datapoints in and around
411 Lomami NP³⁵. Seventh, 23 published locations of savanna, *terra firme* forest, palm- or
412 hardwood-dominated peat swamp forest in DRC¹¹. Eighth, 296 datapoints from
413 Google Earth for unambiguous savanna and water sites (middle of lakes or rivers),
414 distributed across the region.

415

416 We used nine remote sensing products to map peat-associated vegetation
417 (Supplementary Figure 1). Eight of these are identical to those used by Dargie et al.⁹:
418 three optical products (Landsat 7 ETM+ bands 5 [SWIR 1], 4 [NIR], and 3 [Red]); three
419 L-band Synthetic Aperture Radar products (ALOS PALSAR HV, HH, and HV/HH); and
420 two topographic products (SRTM DEM [Digital Elevation Model] void-filled with ASTER
421 GDEM v2 data, and slope; acquisition date 2000). To this, we added a HAND-index
422 (Height Above Nearest Drainage point), which significantly improved model
423 performances (median Matthews correlation coefficient [MCC]: 79.7%, compared with
424 77.8% or 75.6% for just DEM or HAND alone, respectively; $P < 0.001$).

425

426 HAND was derived from the SRTM DEM with Clubb et al.'s algorithm³⁶, using the
427 HydroSHEDS global river network at 15s resolution as reference product³⁷. Alternative
428 NASADEM- or MERIT DEM-derived³⁸⁻⁴⁰ combinations of DEM, HAND and slope were
429 tested with an initial subset of data in R, while keeping all other remote sensing
430 products the same (median MCC: 79.0% and 75.1%, respectively), but did not
431 significantly improve model performance compared with SRTM-derived products
432 (80.9% median MCC; $P < 0.001$).

433

434 The Landsat bands are pre-processed, seamless cloud-free mosaics for ROC
435 (composite of three years, 2000, 2005, 2010) and DRC (composite of six years, 2005-
436 2010)⁴¹. These mosaics performed better than more recent basin-wide automated
437 cloud-free Sentinel-2 mosaics that we developed (bands 5, 8A, 11; composite of five
438 years, 2016-2020), likely because they contain less directional reflectance artefacts
439 (the median MCC of 80.9% for the pre-processed Landsat mosaics is significantly
440 higher than the 78.1% for our Sentinel-2 mosaics, $P < 0.005$).

441

442 The ALOS PALSAR radar bands are mosaics of mean values of annual JAXA
443 composites for the years 2007-2010 (ref. ⁹). More recent radar data (ALOS 2-PALSAR
444 2 HV, HH, HV/HH; 2015-2017) did not significantly improve model performances
445 (median MCC 80.9% and 80.6%, respectively; $P < 0.01$). All remote sensing products
446 were resized to a common 50 m grid, using a cubic convolution resampling method.

447

448 We then tested which classification algorithm to use, as more sophisticated algorithms
449 might improve overall accuracy against our training dataset, but might also reduce
450 regional accuracy of the map in areas far from test data, critical in this case given large
451 areas of the central Congo peatland region remain unsampled.

452

453 Three supervised classification algorithms were tested in order of increasing
454 complexity: Maximum Likelihood (ML), Support Vector Machine (SVM) and Random
455 Forest (RF). We assessed each classifier using both a random and spatial cross-
456 validation (CV) approach⁴²⁻⁴⁴. Random CV was implemented using stratified two-
457 thirds Monte Carlo selection, whereby we 1,000 times randomly selected two-thirds of

458 all datapoints per class as training data, to be evaluated against the remaining one-
459 third per class as testing data.

460

461 Spatial CV was implemented by grouping all transects datapoints in four distinct hydro-
462 geomorphological regions: (i) transects perpendicular to the blackwater Likouala-aux-
463 Herbes River (n = 179 datapoints); (ii) transects perpendicular to the white-water
464 Ubangi River (n = 113); (iii) transects perpendicular to the Congo River, intermediate
465 between black and white-water (n = 123); and (iv) transects perpendicular to the
466 blackwater Ruki, Busira and Ikelemba Rivers, plus other nearby transects (collectively
467 named the Ruki group; n = 258). To each group we added ground-truth datapoints
468 from other non-transect data sources (Supplementary Table 2) that belonged to the
469 same map regions (n = 82, 27, 20, 113, respectively). We then tested 1,000 times how
470 well each classifier performs in each of the four regions, when trained only on a
471 stratified two-thirds Monte Carlo selection of the remaining datapoints (i.e., datapoints
472 from the three other regional transect groups), plus ground-truth datapoints not
473 associated with or near any transect group (n = 821; for example, the savanna and
474 *terra firme* forest datapoints in Lomami National Park in DRC which are far [> 300 km]
475 from any transect group).

476

477 Model performance was based on Matthews correlation coefficient (MCC) for binary
478 peat/non-peat predictions (hardwood- and palm-dominated peat swamp forest classes
479 combined into one peat class; water, savanna and non-peat forming forest combined
480 into one non-peat class). We compared MCC, rather than popular metrics such as
481 Cohen's kappa, F1-score or accuracy, because it is thought to be the most reliable
482 evaluation metric for binary classifications^{45,46}. We also computed balanced accuracy

483 (BA) from random cross-validation to compare with the first-generation map. While
484 less robust than MCC, BA is independent of imbalances in the prevalence of
485 positives/negatives in the data, thus allowing better comparison between classifiers
486 trained on different datasets¹⁶. The best estimate of each accuracy metric or area
487 estimate per model or region is the median value of 1,000 runs, alongside a 95%
488 confidence interval.

489

490 In the case of SVM and RF, random CV models were implemented in Google Earth
491 Engine (GEE)⁴⁷ using all nine remote sensing products. However, because ML is
492 currently not supported by GEE, random CV with this algorithm was implemented in
493 IDL-ENVI software (version 8.7-5.5), using a principal component analysis (PCA) to
494 reduce the nine remote sensing products to six uncorrelated principal components to
495 reduce computation time. All spatial CV models were implemented in R (*superClass*
496 function from the *RStoolbox* package, version 0.2.6), with PCA also applied in the case
497 of ML only. All RF models were trained using 500 trees, with three input products used
498 at each split in the forest (the default, the square root of the number of variables). All
499 SVM model were implemented with a radial basis function kernel, with all other
500 parameters set to default values.

501

502 Comparison of the ML, SVM and RF models with Dargie et al.'s model performance⁹,
503 using balanced accuracy from random cross-validation, shows improved results only
504 in the case of the ML classifier (Supplementary Table 3). Comparing MCC using the
505 spatial CV approach, we found that the ML algorithm is also most transferable to
506 regions for which we lack training data. While RF gives slightly better MCC with
507 random CV, when no regions are omitted, spatial CV shows particularly poor predictive

508 performance of this algorithm for the Congo and Ruki regions, when trained on data
509 from the other regions. SVM has lowest MCC of all three classifiers with random CV,
510 and also performs worst of all three in the Congo region with spatial CV.

511

512 Additionally, applying spatial CV to the largely interfluvial basin region (ROC transects;
513 $n = 401$), and the largely river-influenced region (DRC transects; $n = 540$), also shows
514 RF performs poorly (Supplementary Table 3). This further supports selecting the ML
515 algorithm to produce our second-generation peat extent map of the central Congo
516 peatlands. The final peatland extent estimate is then obtained as the median value
517 (alongside 95% confidence interval) out of the combined hardwood- and palm-
518 dominated peat swamp forest extent from 1,000 ML runs, each time trained with two-
519 thirds of the ground-truth data.

520

521 ***Modelling peat thickness***

522 A map of distance from the peatland margins was developed in GEE using the median
523 ML peat probability map, i.e. the ML map with a 50% peat probability threshold (> 500
524 hardwood- or palm-dominated peat swamp predictions out of 1,000 runs). For each
525 peat pixel in this binary classification, a cost function was used to calculate the
526 Euclidean distance to the nearest non-peat pixel, after speckle and noise were
527 removed using a 5x5 squared-kernel majority filter. Using this distance map, transects
528 were found to have markedly different relationships between peat thickness and
529 distance from the peatland margin, i.e. different slopes ($n = 18$, $P < 0.001$, Extended
530 Data Figure 4). The modest linear fit ($R^2 = 41.0\%$; $RMSE = 1.21$ m) cautions against
531 a uniform regression between peat thickness and distance from the margin across the
532 basin.

533

534 Instead, we developed a spatially-explicit Random Forest regression model to predict
535 peat thickness, derived from 14 remotely-sensed potential covariates that may explain
536 variation in peat thickness. These 14 variables included the nine optical, radar and
537 topographic products used in the peatland extent analysis, as well as distance from
538 the peatland margin, distance from the nearest drainage point (same reference
539 network as for HAND)³⁷, precipitation seasonality⁴⁸, climatic water balance (mean
540 annual precipitation⁴⁸ minus mean annual potential evapotranspiration⁴⁹), and live
541 woody aboveground biomass⁵⁰. Ten of these variables were found to be significantly
542 correlated with peat thickness (Kendall's τ , $P < 0.01$): all three optical bands, all three
543 radar bands, distance from the peatland margin, distance from the nearest drainage
544 point, precipitation seasonality, and climatic water balance. Applying stepwise
545 backward selection, we tested combinations of these ten predictors by each time
546 dropping one predictor out of the model in order from low to high variable importance,
547 selecting as the best model the one with highest median R^2 and lowest median root
548 mean square error (RMSE) obtained from 100 random (two-thirds) cross-validations.
549 The importance of each variable was assessed by calculating Mean Decrease Impurity
550 (MDI), the total decrease in the residual sum of squares of the regression after splitting
551 on that variable, averaged over all decision trees in the random forest. Median MDI
552 was calculated for each variable based on 100 random (two-thirds) cross-validations
553 of the overall model containing all ten significant predictors.

554

555 The best model contained four predictors: distance from the peatland margin, distance
556 to the nearest drainage point, climatic water balance (all positively correlated with peat
557 thickness; Kendall's τ coefficient = 0.49, 0.15 and 0.13, respectively; $P < 0.001$ for all),

558 and precipitation seasonality (negatively correlated with thickness; Kendall's $\tau = -0.11$,
559 $P < 0.01$); see Extended Data Figure 6 for their spatial variability.

560

561 The RF regression was implemented in GEE with 500 trees and all other parameters
562 set to default values. Predictor variables were resampled to 50 m resolution. As
563 training data, we included all LOI-verified and corrected pole-method thickness
564 measurements that fell within the masked map of $> 50\%$ peat probability ($n = 463$),
565 including thickness > 0 and < 0.3 m from non-peat sites that could improve predictions
566 of shallow peat deposits near the margins ($n = 12$).

567

568 Our final RF model ($R^2 = 93.4\%$, RMSE = 0.42 m) had consistently smaller residuals
569 compared to a multiple linear regression model containing the same four predictors
570 with interaction effects ($\text{adj-}R^2 = 73.6\%$, RMSE = 0.80 m; Extended Data Figure 5). It
571 also performed better when testing out-of-sample performance, using 100 random
572 two-thirds cross-validations of training data (median $R^2 = 82.2\%$, RMSE = 0.68 m; and
573 median $\text{adj-}R^2 = 73.6\%$, RMSE = 0.85 m; for RF model and multiple linear regression,
574 respectively).

575

576 For uncertainty on our thickness predictions, we first estimated area uncertainty by
577 creating 100 different maps of distance from the peat margin, by randomly selecting
578 (with replacement) a minimum peat probability threshold $> 0\%$ and $< 100\%$, removing
579 speckle and noise, and re-calculating the closest distance to the nearest non-peat
580 pixel. We then combined the 100 distance maps each time with the three other
581 selected predictors (precipitation seasonality, climatic water balance, distance from
582 nearest drainage point) as input in a RF model to develop 100 different peat thickness

583 maps. For these model runs, we included all available thickness measurements (> 0
584 m) that fell within each specific distance map. Each output map was masked to an
585 area ≥ 0.3 m thickness, consistent with our peat definition. A map of median peat
586 thickness (Figure 3a) and relative uncertainty (\pm half the width of the 95% CI as
587 percentage of the median; Figure 3b) was then calculated for each pixel based on the
588 100 available thickness estimates.

589

590 ***Carbon stock estimates***

591 We mapped carbon density across the central Congo Basin in GEE, by applying 20
592 bootstrapped thickness-carbon regressions that were normally distributed around the
593 best fit (Extended Data Figure 7 6) to the 100 peat thickness maps from the RF
594 regression model, generating a map of median carbon density out of 2,000 estimates
595 (Figure 3a), together with relative uncertainty (\pm half the width of the 95% CI as
596 percentage of the median; Figure 3b).

597

598 Total peat carbon stocks were computed in GEE by summing carbon density (in Mg
599 ha^{-1}) over all 50 m grid squares defined as peat. To assess uncertainty around this
600 estimate, we again combined the 100 peat thickness maps (i.e., uncertainty from area
601 and thickness), with 20 bootstrapped thickness-carbon regressions (i.e., uncertainty
602 from carbon density, including bulk density and carbon concentration). We thus
603 obtained 2,000 peat carbon stock estimates for the total central Congo Basin peatland
604 complex, which were used to estimate the mean, median and 95% CI (Extended Data
605 Figure 8a).

606

607 Regional carbon stock estimates were similarly obtained for each sub-national
608 administrative region (departments in ROC and provinces in DRC; Extended Data
609 Figure 2), as well as national-level protected areas (national parks and
610 nature/biosphere/community reserves)⁵¹ and logging^{52,53}, mining^{54,55} and palm oil^{56–58}
611 concessions (Extended Data Figures 9 and 10). As hydrocarbon concessions cover
612 almost the whole peatlands area^{24,26}, they cover almost 100% of the central Congo
613 peat carbon stocks.

614

615 Sensitivity analysis was performed by bootstrapping either the area, thickness, or
616 carbon density component, whilst keeping the others constant (Extended Data Figure
617 8b). For area, we bootstrapped 100 randomly selected peatland area estimates; for
618 thickness, 100 randomly selected two-thirds subsets of all thickness measurements;
619 for carbon density, 20 normally distributed regression equations from the bootstrapped
620 thickness-carbon relationship.

621

622 **DATA AVAILABILITY**

623 All map results from this study are available for download as raster files from
624 <https://congopeat.net/maps/>. The supporting ground-truth data, peat thickness
625 measurements, and carbon density measurements are available from
626 <https://github.com/CongoPeat/Peatland-mapping.git> . The remote sensing datasets
627 used are available for download from
628 https://www.eorc.jaxa.jp/ALOS/en/dataset/fnf_e.htm (ALOS PALSAR and ALOS-2
629 PALSAR-2 25 m HV and HH data), <http://osfac.net/> (OSFAC ROC and DRC 60 m
630 Landsat ETM+ bands 5, 4 and 3 mosaics), and <http://earthexplorer.usgs.gov/> (SRTM
631 DEM 1-arc second and ASTER GDEM v2 1-arc second data).

632

633

634 **CODE AVAILABILITY**

635 The IDL-ENVI script to run the Maximum Likelihood peatland extent model is
636 available from <https://github.com/CongoPeat/Peatland-mapping.git>. The scripts to
637 run the peat thickness model and carbon stock calculations are available on Google
638 Earth Engine:
639 [https://code.earthengine.google.com/?accept_repo=users/gybjc/Central Congo Pea](https://code.earthengine.google.com/?accept_repo=users/gybjc/Central_Congo_Pea)
640 [tlands_2022](#). All R code is available from the corresponding author upon request.

641

642 **ACKNOWLEDGEMENTS**

643 We sincerely thank the communities that hosted and assisted with our fieldwork in
644 DRC: Lokolama, Bosukela, Mpama, Befale, Bonsole, Mweko, Mpeka, Bondamba,
645 Bolengo, Boleke, Pombi, Boboka, Ipombo, Lobaka, Bolombo, and Bonzembo. We
646 thank the Groupe d'action pour sauver l'homme et son environnement (GASHE),
647 especially Julien Mathe, and Greenpeace Africa, especially Raoul Monsembula, for
648 essential logistical support. We thank the government of the Democratic Republic of
649 the Congo, the Province of Équateur, and the Ministry of Environment and Sustainable
650 Development for assistance with our fieldwork. We thank Bolivard Bongwemisa,
651 Juress Sando, Jean-Pierre Lokila, Papy Bosange, Felly Mongonga and Roger
652 Kendewa for essential field support. David Milodowski and Adam Hastie provided
653 modelling advice, Rachel Gasior, David Ashley, Martin Gilpin and Dave Wilson
654 provided laboratory assistance, and Donna Hawthorne, George Biddulph, Shona
655 Jenkins, Sofie Sjögersten, Guy Ziv and the CongoPeat network provided invaluable
656 discussions and feedback. The work was funded by a NERC Large Grant to S.L.L.
657 (“CongoPeat”, NE/R016860/1), a NERC Doctoral Training Partnership award to B.C.
658 (“SPHERES DTP”, NE/L002574/1), and a Greenpeace Fund award to S.L.L.. JAXA,
659 NASA, METI, USGS, ESA, OSFAC, and WWF are acknowledged for collecting and/or
660 processing remote sensing data.

661

662 **AUTHOR CONTRIBUTIONS**

663 S.L.L., E.T.A.M., I.T.L., G.C.D., and S.E.P. conceived the study; B.C., G.C.D., S.L.L.,
664 E.T.A.M., I.T.L., S.E.P., S.A.I., C.E.N.E. and T.R.B. developed the study; B.C., G.C.D.,
665 S.L.L. C.E.N.E., O.E.B., P.B., J.K.T., N.T.G., and J-B.N.N. organised and conducted
666 the fieldwork; Y.E.B., S.A.I., W.H., D.S., R.B., G.I., A.C-S., C.A.K., J.L. and H-P.W.
667 provided additional data; B.C., G.C.D., A.B. and H.B. performed laboratory analyses;
668 B.C. and E.T.A.M. analysed the remote sensing data and developed the models; B.C.,
669 S.L.L., E.T.A.M., G.C.D., A.J.B., T.R.B., P.J.M. and C.A.K. evaluated the results. B.C.
670 and S.L.L. wrote the paper, with input from all co-authors.

671

672 **COMPETING INTERESTS**

673 The authors declare no competing interests.

674

675 **TABLES**

676

677 **Table 1 | Field-measured and spatially modelled estimates of peat thickness, bulk density, carbon concentration, and**678 **carbon density in the central Congo Basin peatland complex.**

	Field measurements *														Spatial model †					
	Peat thickness (m) #			Peat bulk density (g cm ⁻³) §				Peat carbon concentration (%) ‡				Peat carbon density (Mg C ha ⁻¹) ‡			Peat thickness (m) ¶			Peat carbon density (Mg C ha ⁻¹) §		
	Mean ± s.d.	Median	Max	Mean ± s.d.	Median	Min	Max	Mean ± s.d.	Median	Min	Max	Mean ± s.d.	Median	Max	Mean ± s.d.	Median	Max	Mean ± s.d.	Median	Max
Interfluvial basin peatlands (ROC)	2.4 (1.5)	2.1	5.9	0.19 (0.06)	0.19	0.10	0.31	56.2 (2.7)	56.5	49.6	61.8	1,619 (810)	1,640	3,183	1.7 (0.9)	1.3	5.4	1,653 (687)	1,402	3,852
River-influenced peatlands (DRC)	2.4 (1.6)	2.0	6.4	0.15 (0.07)	0.15	0.02	0.33	55.0 (3.6)	55.8	42.0	59.2	1,883 (1,511)	1,762	5,162	1.8 (0.8)	1.6	5.6	1,740 (604)	1,697	3,970
Central Congo Basin peatlands (ROC + DRC)	2.4 (1.5)	2.0	6.4	0.17 (0.06)	0.17	0.02	0.33	55.7 (3.2)	56.3	42.0	61.8	1,741 (1,186)	1,700	5,162	1.7 (0.9)	1.6	5.6	1,712 (634)	1,661	3,970

679 * Field measurement statistics include either the Likouala-aux-Herbes and Ubangi River groups of transects only ('Interfluvial
680 basin peatlands'), or the Congo and Ruki River groups of transects only ('River-influenced peatlands'), or all groups ('Central
681 Congo Basin peatlands').

682 † Spatial model statistics include all 50 m resolution pixels mapped in either Republic of the Congo only (ROC), Democratic
683 Republic of the Congo only (DRC), or both countries (ROC + DRC).

684 # In situ measurements (laboratory and corrected pole-methods) from 213, 238 and 451 locations in ROC (ref. ⁹), DRC (this
685 study) and combined, respectively. Peat is ≥ 0.3 m thickness and $\geq 65\%$ organic matter.

686 § $n = 43, 37,$ and 80 well-sampled cores in ROC (ref. ⁹), DRC (this study) and combined, respectively, based on 0.1-m thick
687 samples.

688 ‡ $n = 43, 37,$ and 80 well-sampled and interpolated cores in ROC (ref. ⁹), DRC (this study) and combined, respectively, based
689 on 0.1-m thick samples.

690 ¶ Median estimate from 100 thickness estimates per 50 m resolution pixel across the median extent map, with thickness
691 estimated from 100 RF regression models trained with four predictor variables, each with a randomly selected Maximum
692 Likelihood peat probability threshold to derive distance from the peatland margin.

693 \$ Median estimate from 2,000 carbon density estimates per 50 m resolution pixel across the median peat area map, with
694 carbon density estimates derived from 20 normally distributed thickness-carbon regressions (Extended Data Figure 7) applied
695 to 100 peat thickness estimates.

696 **FIGURE LEGENDS/CAPTIONS**

697

698 **Figure 1: Maps of field sampling locations (a), peat swamp forest predictions**
699 **from this study (b), and a comparison of our predictions with a previous map⁹**

700 **(c).** **a**, Points indicate transects, coloured by region. The Congo and Ruki River
701 regional groups appear to be in largely river-influenced peatlands, predominating in
702 DRC, sampled for this study. The Likouala-aux-Herbes and Ubangi River regional
703 groups are in largely rain-fed interfluvial basins, predominating in ROC, from Ref. ⁹.
704 The base map, in green, shows the first-generation peat swamp forest map⁹. Inset:
705 Location of central Congo Basin peatlands. **b**, Predicted landcover classes across the
706 central Congo Basin as the most likely class per pixel (>50%), using a legend identical
707 to Ref. ⁹ to facilitate comparison. **c**, Peat swamp forest predictions from this study and
708 Ref. ⁹ using the most likely class per pixel. White indicates peat in both studies; red
709 indicates peat in this study only; blue indicates peat only in Ref. ⁹. Open water is dark
710 grey. In all panels, national boundaries are black lines; sub-national boundaries are
711 grey lines; non-peat forming forest includes both *terra firme* and non-peat forming
712 seasonally inundated forests.

713

714 **Figure 2: Maps of peat thickness and uncertainty across the central Congo**

715 **Basin.** **a**, Median prediction of peat thickness (m) from 100 Random Forest regression
716 models with four predictors: distance from the peatland margin, precipitation
717 seasonality, climatic water balance, and distance from the nearest drainage point. **b**,
718 Relative uncertainty (%) of the peat thickness estimate, expressed as \pm half the width
719 of the 95% confidence interval as percentage of the median. Black lines represent
720 national boundaries; grey lines represent sub-national administrative boundaries.

721

722 **Figure 3: Maps of belowground peat carbon density and uncertainty across the**
723 **central Congo Basin. a**, Median prediction of belowground peat carbon density (Mg
724 C ha⁻¹), obtained from applying 20 normally distributed thickness-carbon density
725 regressions (Extended Data Figure 7) to 100 peat thickness estimates (Figure 2a),
726 generating 2,000 carbon density estimates. **b**, Relative uncertainty (%) of the carbon
727 density estimate, expressed as \pm half the width of the 95% confidence interval as
728 percentage of the median. Black lines represent national boundaries; grey lines
729 represent sub-national administrative boundaries.

730

731 **REFERENCES**

- 732 1. Xu, J., Morris, P. J., Liu, J. & Holden, J. PEATMAP: Refining estimates of
733 global peatland distribution based on a meta-analysis. *Catena* **160**, 134–140
734 (2018).
- 735 2. Yu, Z., Loisel, J., Brosseau, D. P., Beilman, D. W. & Hunt, S. J. Global
736 peatland dynamics since the Last Glacial Maximum. *Geophys. Res. Lett.* **37**,
737 1–5 (2010).
- 738 3. Leifeld, J. & Menichetti, L. The underappreciated potential of peatlands in
739 global climate change mitigation strategies. *Nat. Commun.* **9**, 1–7 (2018).
- 740 4. Scharlemann, J. P. W., Tanner, E. V. J., Hiederer, R. & Kapos, V. Global soil
741 carbon: understanding and managing the largest terrestrial carbon pool.
742 *Carbon Manag.* **5**, 81–91 (2014).
- 743 5. Page, S. E., Rieley, J. O. & Banks, C. J. Global and regional importance of the
744 tropical peatland carbon pool. *Glob. Chang. Biol.* **17**, 798–818 (2011).
- 745 6. Ribeiro, K. *et al.* Tropical peatlands and their contribution to the global carbon
746 cycle and climate change. *Glob. Chang. Biol.* **00**, 1–17 (2020).
- 747 7. Leifeld, J., Wüst-Galley, C. & Page, S. Intact and managed peatland soils as a
748 source and sink of GHGs from 1850 to 2100. *Nat. Clim. Chang.* **9**, 945–947
749 (2019).
- 750 8. Page, S. E. *et al.* The amount of carbon released from peat and forest fires in
751 Indonesia during 1997. *Nature* **420**, 61–65 (2002).
- 752 9. Dargie, G. C. *et al.* Age, extent and carbon storage of the central Congo Basin
753 peatland complex. *Nature* **542**, 86–90 (2017).

- 754 10. Alsdorf, D. *et al.* Opportunities for hydrologic research in the Congo Basin.
755 *Rev. Geophys.* **54**, 378–409 (2016).
- 756 11. Kiahtipes, C. A. & Schefuß, E. Congo Basin peatlands as a baseline record for
757 past hydrology and climate [W-68]. *Earth Sp. Sci. Open Arch.* (2019)
758 doi:<https://www.essoar.org/doi/10.1002/essoar.10500726.1>.
- 759 12. Davenport, I. J. *et al.* First Evidence of Peat Domes in the Congo Basin using
760 LiDAR from a Fixed-Wing Drone. *Remote Sens.* **12**, 1–13 (2020).
- 761 13. Lee, H. *et al.* Characterization of terrestrial water dynamics in the Congo Basin
762 using GRACE and satellite radar altimetry. *Remote Sens. Environ.* **115**, 3530–
763 3538 (2011).
- 764 14. Rosenqvist, A. Mapping of seasonal inundation in the Congo River basin -
765 Prototype study using ALOS PALSAR. *Proc. 33rd Int. Symp. Remote Sens.*
766 *Environ. ISRSE* **33**, 709–712 (2009).
- 767 15. Lee, H., Yuan, T., Jung, H. C. & Beighley, E. Mapping wetland water depths
768 over the central Congo Basin using PALSAR ScanSAR, Envisat altimetry, and
769 MODIS VCF data. *Remote Sens. Environ.* **159**, 70–79 (2015).
- 770 16. Chicco, D., Tötsch, N. & Jurman, G. The Matthews correlation coefficient
771 (MCC) is more reliable than balanced accuracy, bookmaker informedness, and
772 markedness in two-class confusion matrix evaluation. *BioData Min.* **14**, 1–22
773 (2021).
- 774 17. Gumbricht, T. *et al.* An expert system model for mapping tropical wetlands and
775 peatlands reveals South America as the largest contributor. *Glob. Chang. Biol.*
776 **23**, 3581–3599 (2017).

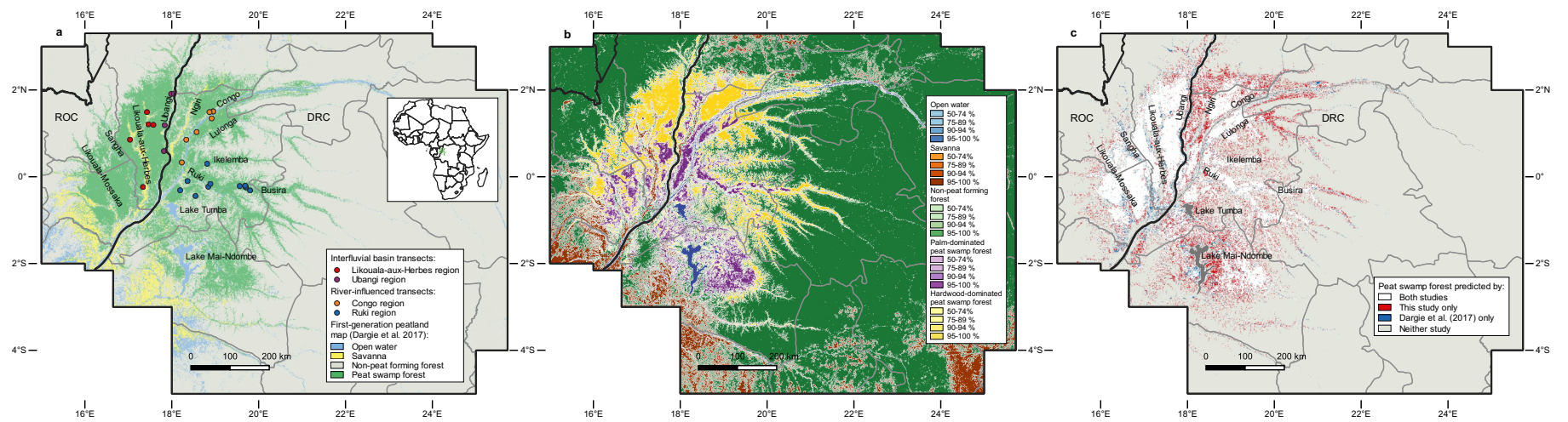
- 777 18. Young, D. M., Parry, L. E., Lee, D. & Ray, S. Spatial models with covariates
778 improve estimates of peat depth in blanket peatlands. *PLoS One* **13**, 1–19
779 (2018).
- 780 19. Rudiyanto *et al.* Digital mapping for cost-effective and accurate prediction of
781 the depth and carbon stocks in Indonesian peatlands. *Geoderma* **272**, 20–31
782 (2016).
- 783 20. Malhi, Y. & Wright, J. Spatial patterns and recent trends in the climate of
784 tropical rainforest regions. *Philos. Trans. R. Soc. B Biol. Sci.* **359**, 311–329
785 (2004).
- 786 21. Lewis, S. L. *et al.* Above-ground biomass and structure of 260 African tropical
787 forests. *Philos. Trans. R. Soc. B Biol. Sci.* **368**, 1–14 (2013).
- 788 22. Hastie, A. *et al.* Risks to carbon storage from land-use change revealed by
789 peat thickness maps of Peru. *Nat. Geosci.* (2022)
790 doi:<https://doi.org/10.1038/s41561-022-00923-4>.
- 791 23. Verhegghen, A., Mayaux, P., De Wasseige, C. & Defourny, P. Mapping Congo
792 Basin vegetation types from 300 m and 1 km multi-sensor time series for
793 carbon stocks and forest areas estimation. *Biogeosciences* **9**, 5061–5079
794 (2012).
- 795 24. Miles, L. *et al.* Carbon, biodiversity and land-use in the Central Congo Basin
796 Peatlands. *UN Environment Programme* (2017).
- 797 25. Vancutsem, C. *et al.* Long-term (1990–2019) monitoring of forest cover
798 changes in the humid tropics. *Sci. Adv.* **7**, 1–21 (2021).
- 799 26. Dargie, G. C. *et al.* Congo Basin peatlands: threats and conservation priorities.

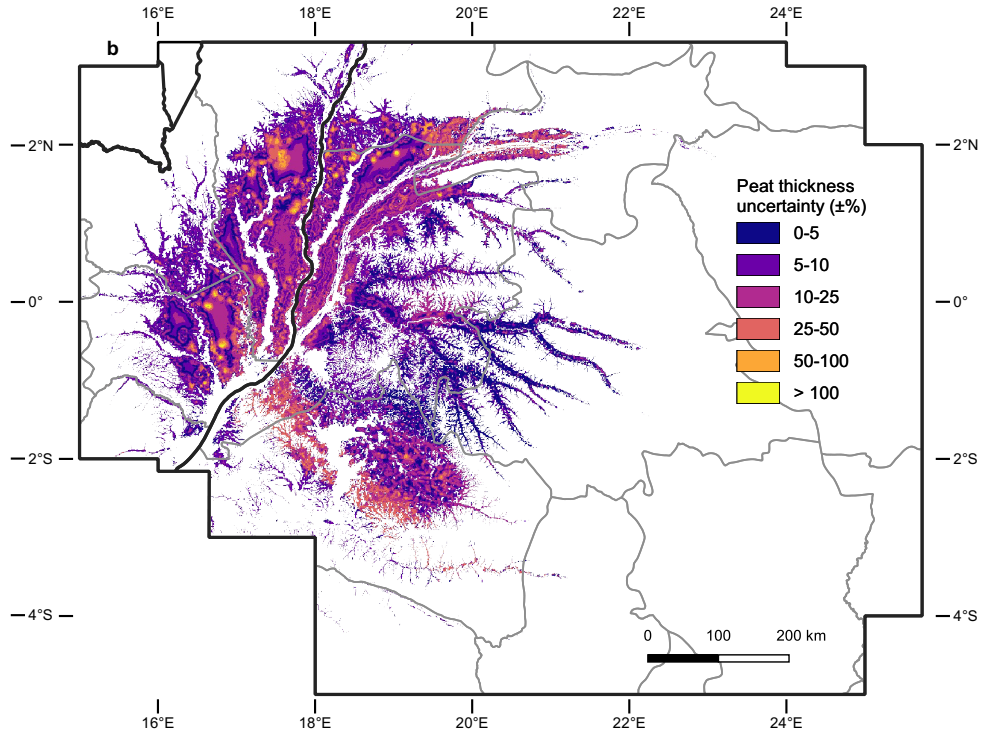
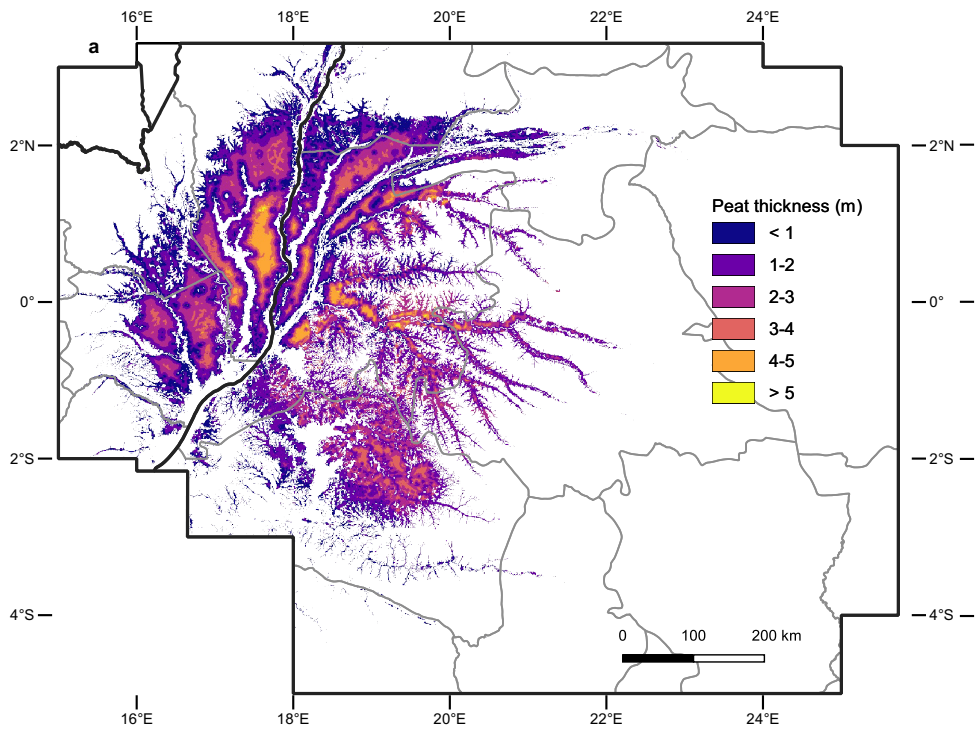
- 800 *Mitig. Adapt. Strateg. Glob. Chang.* **24**, 669–686 (2018).
- 801 27. Maisels, F. *et al.* Devastating Decline of Forest Elephants in Central Africa.
802 *PLoS One* **8**, 1–13 (2013).
- 803 28. Strindberg, S. *et al.* Guns, germs, and trees determine density and distribution
804 of gorillas and chimpanzees in Western Equatorial Africa. *Sci. Adv.* **4**, 1–14
805 (2018).
- 806 29. Lawson, I. T. *et al.* Improving estimates of tropical peatland area, carbon
807 storage, and greenhouse gas fluxes. *Wetl. Ecol. Manag.* **23**, 327–346 (2015).
- 808 30. Seidensticker, D. *et al.* Population collapse in Congo rainforest from 400 CE
809 urges reassessment of the Bantu Expansion. *Sci. Adv.* **7**, 1–13 (2021).
- 810 31. Seidensticker, D. dirkseidensticker/HumActCentralAfrica_Paper: Codebase
811 (Version v1.0). *Zenodo* (2020) doi:10.5281/ZENODO.4394894.
- 812 32. Hubau, W. *et al.* Asynchronous carbon sink saturation in African and
813 Amazonian tropical forests. *Nature* **579**, 80–87 (2020).
- 814 33. Lopez-Gonzalez, G., Lewis, S. L., Burkitt, M., Baker, T. R. & Phillips, O. L.
815 ForestPlots.net Database. www.forestplots.net (2009).
- 816 34. Lopez-Gonzalez, G., Lewis, S. L., Burkitt, M. & Phillips, O. L. ForestPlots.net:
817 A web application and research tool to manage and analyse tropical forest plot
818 data. *J. Veg. Sci.* **22**, 610–613 (2011).
- 819 35. Batumike, R., Imani, G., Urom, C. & Cuni-Sanchez, A. Bushmeat hunting
820 around Lomami National Park, Democratic Republic of the Congo. *Oryx* **55**, 1–
821 11 (2020).

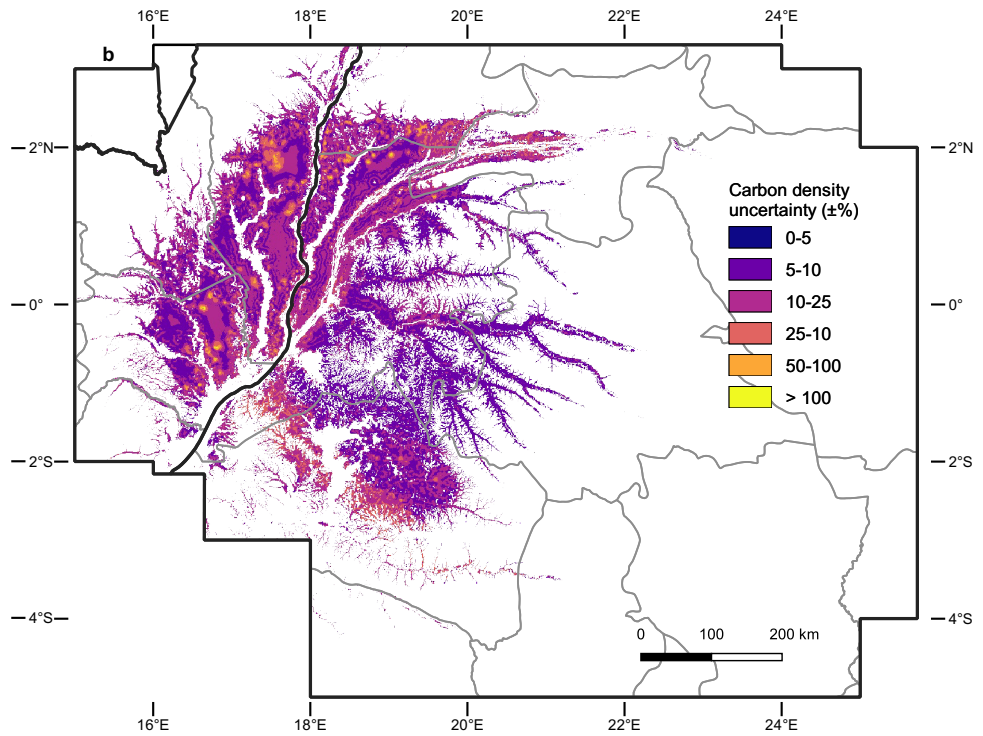
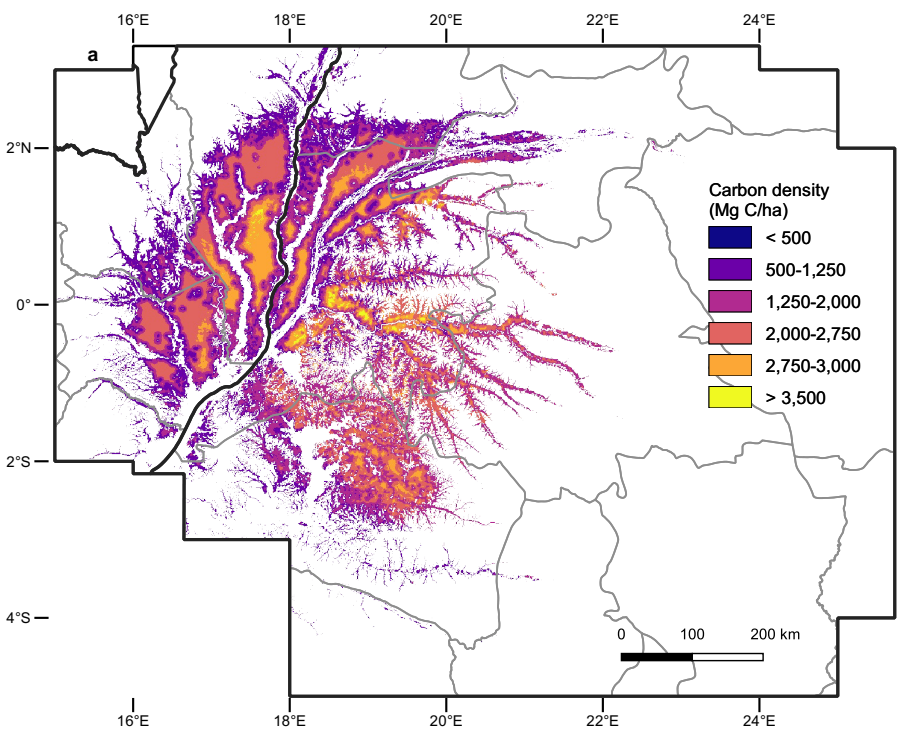
- 822 36. Clubb, F. J. *et al.* Geomorphometric delineation of floodplains and terraces
823 from objectively defined topographic thresholds. *Earth Surf. Dyn.* **5**, 369–385
824 (2017).
- 825 37. Lehner, B., Verdin, K. & Jarvis, A. New Global Hydrography Derived From
826 Spaceborne Elevation Data. *Eos, Trans. Am. Geophys. Union* **89**, 93–94
827 (2008).
- 828 38. NASA Jet Propulsion Laboratory. NASADEM Merged DEM Global 1 arc
829 second V001. (2020)
830 doi:https://doi.org/10.5067/MEaSURES/NASADEM/NASADEM_HGT.001.
- 831 39. Yamazaki, D. *et al.* A high-accuracy map of global terrain elevations. *Geophys.*
832 *Res. Lett.* **44**, 5844–5853 (2017).
- 833 40. Yamazaki, D. *et al.* MERIT Hydro : A High-Resolution Global Hydrography Map
834 Based on Latest Topography Dataset. *Water Resour. Res.* **55**, 5053–5073
835 (2019).
- 836 41. Observatoire Satellital des Forêts d’Afrique Centrale (OSFAC). Forêts
837 d’Afrique Centrale Evaluées par Télédétection. [https://osfac.net/data-](https://osfac.net/data-products/facet/)
838 [products/facet/](https://osfac.net/data-products/facet/) (2014).
- 839 42. Ploton, P. *et al.* Spatial validation reveals poor predictive performance of large-
840 scale ecological mapping models. *Nat. Commun.* **11**, 1–11 (2020).
- 841 43. Roberts, D. R. *et al.* Cross-validation strategies for data with temporal, spatial,
842 hierarchical, or phylogenetic structure. *Ecography (Cop.)*. **40**, 913–929 (2017).
- 843 44. Meyer, H., Reudenbach, C., Wöllauer, S. & Nauss, T. Importance of spatial
844 predictor variable selection in machine learning applications – Moving from

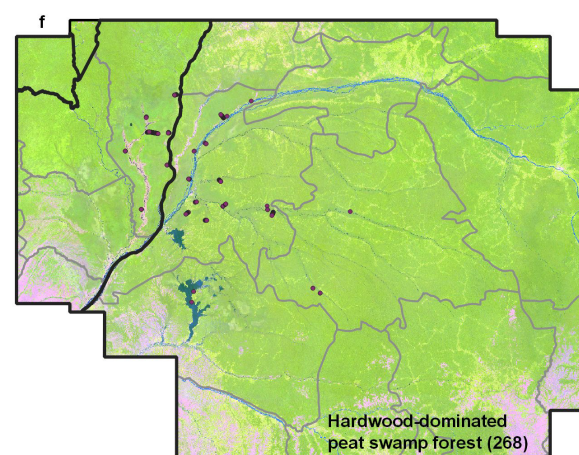
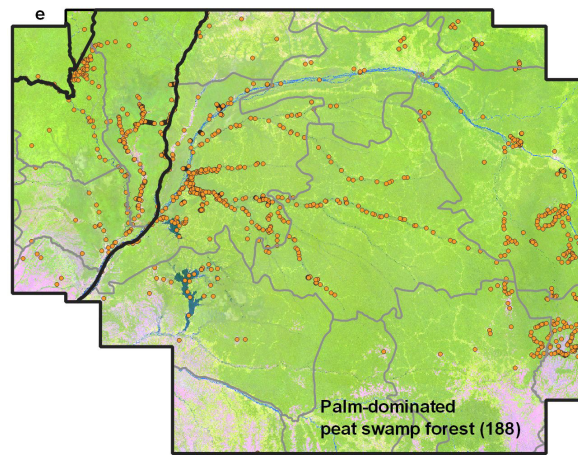
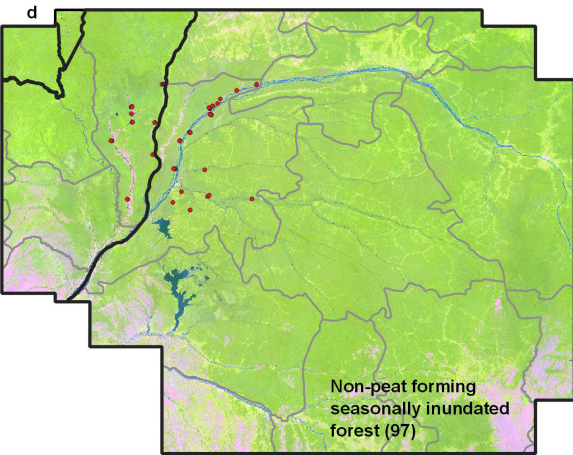
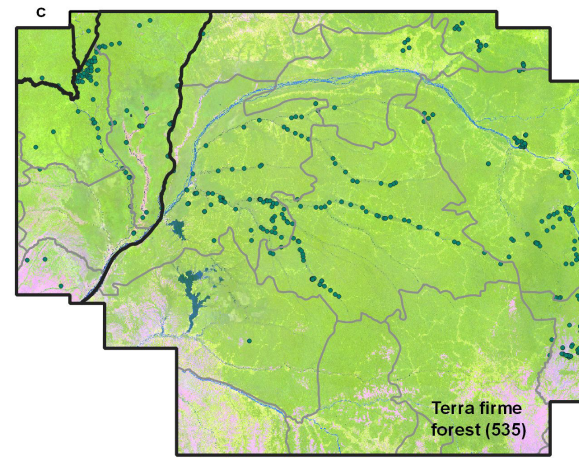
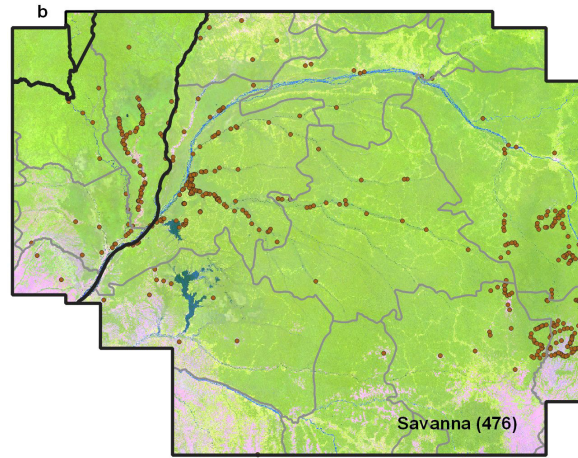
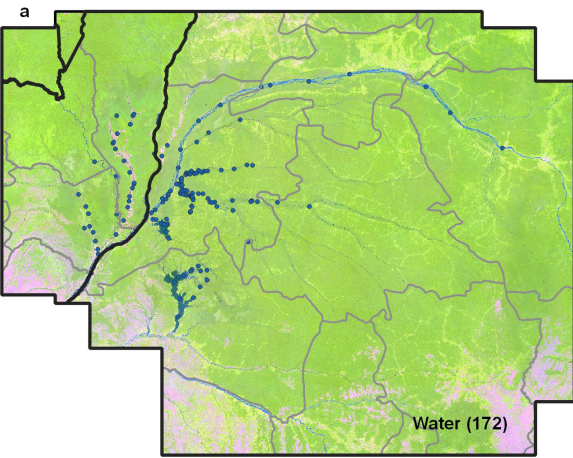
- 845 data reproduction to spatial prediction. *Ecol. Modell.* **411**, 11 (2019).
- 846 45. Chicco, D. & Jurman, G. The advantages of the Matthews correlation
847 coefficient (MCC) over F1 score and accuracy in binary classification
848 evaluation. *BMC Genomics* **21**, 1–13 (2020).
- 849 46. Powers, D. M. W. Evaluation: From Precision, Recall and F-Measure to ROC,
850 Informedness, Markedness and Correlation. *J. Mach. Learn. Technol.* **2**, 37–63
851 (2011).
- 852 47. Gorelick, N. *et al.* Google Earth Engine: Planetary-scale geospatial analysis for
853 everyone. *Remote Sens. Environ.* **202**, 18–27 (2017).
- 854 48. Fick, S. E. & Hijmans, R. J. WorldClim 2: new 1-km spatial resolution climate
855 surfaces for global land areas. *Int. J. Climatol.* **37**, 4302–4315 (2017).
- 856 49. Trabucco, A. & Zomer, R. J. Global Aridity Index and Potential
857 Evapotranspiration (ET₀) Climate Database v2. *figshare* (2019)
858 doi:<https://doi.org/10.6084/m9.figshare.7504448.v3>.
- 859 50. Baccini, A. *et al.* Estimated carbon dioxide emissions from tropical
860 deforestation improved by carbon-density maps. *Nat. Clim. Chang.* **2**, 182–185
861 (2012).
- 862 51. Protected Planet: The World Database on Protected Areas (WDPA) and World
863 Database on Other Effective Area-based Conservation Measures (WD-
864 OECM). *UNEP-WCMC/IUCN* <https://www.protectedplanet.net> (2021).
- 865 52. Republic of the Congo logging concessions. *Global Forest Watch*
866 [https://data.globalforestwatch.org/datasets/gfw::republic-of-the-congo-logging-](https://data.globalforestwatch.org/datasets/gfw::republic-of-the-congo-logging-concessions/)
867 [concessions/](https://data.globalforestwatch.org/datasets/gfw::republic-of-the-congo-logging-concessions/) (2019).

- 868 53. Democratic Republic of the Congo forest titles. *Global Forest Watch*
869 <https://data.globalforestwatch.org/datasets/535eb1335c4841b0bff272b78e2cc>
870 [2f4_6](https://data.globalforestwatch.org/datasets/535eb1335c4841b0bff272b78e2cc) (2019).
- 871 54. Republic of the Congo mining permits. *Global Forest Watch*
872 <https://data.globalforestwatch.org/datasets/84fbbcc10c9f47f890750dd42426cb>
873 [d2_18/](https://data.globalforestwatch.org/datasets/84fbbcc10c9f47f890750dd42426cb) (2019).
- 874 55. Democratic Republic of the Congo mining permits. *Global Forest Watch*
875 <https://data.globalforestwatch.org/datasets/3b4c0c91306c47abaec0c3fd46088>
876 [242_5/](https://data.globalforestwatch.org/datasets/3b4c0c91306c47abaec0c3fd46088) (2019).
- 877 56. DRC Agriculture Plantations. *MapforEnvironment*
878 <https://mapforenvironment.org/layer/info/80/#5.24/-1.263/19.467> (2014).
- 879 57. Republic of the Congo oil palm concessions. *Global Forest Watch*
880 <https://data.globalforestwatch.org/datasets/f1fb5773903244abbe8282cae1898>
881 [63e_17/](https://data.globalforestwatch.org/datasets/f1fb5773903244abbe8282cae1898) (2019).
- 882 58. The Coming Storm: How Secrecy and Collusion in Industrial Agriculture Spell
883 Disaster for the Congo Basin's Forests. *Earthsight*
884 <https://www.earthsight.org.uk/news/investigations/the-coming-storm> (2018).
885

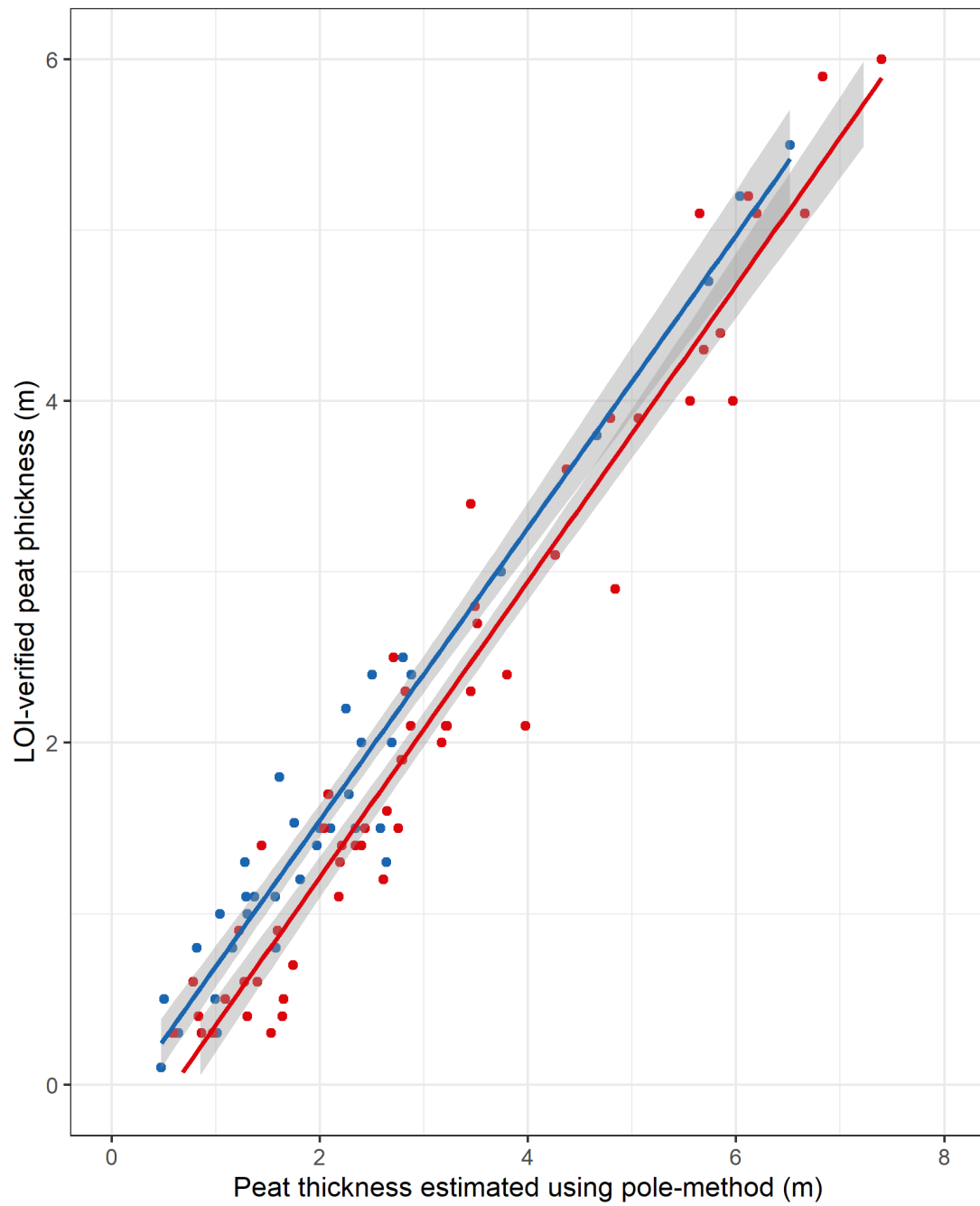






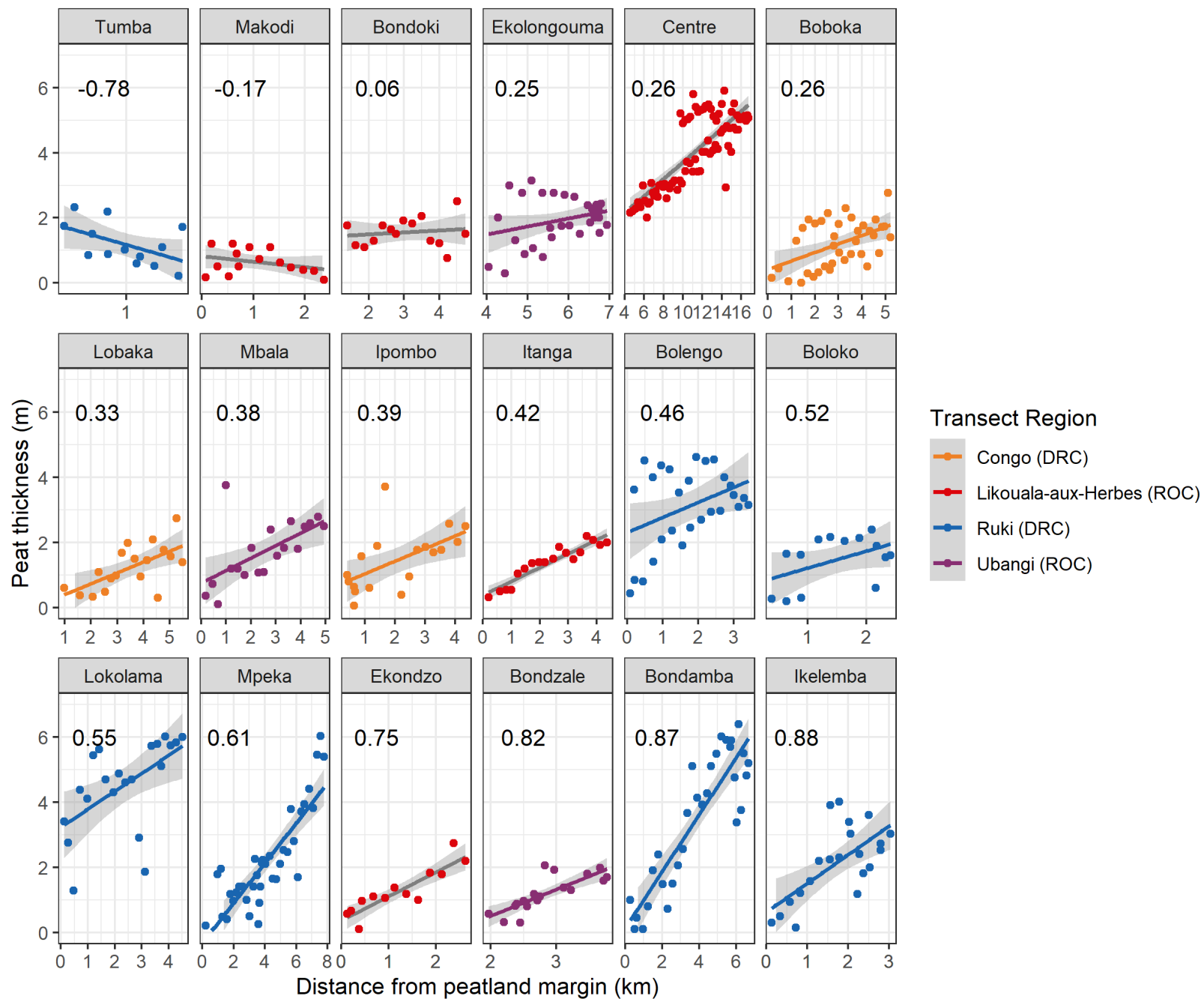


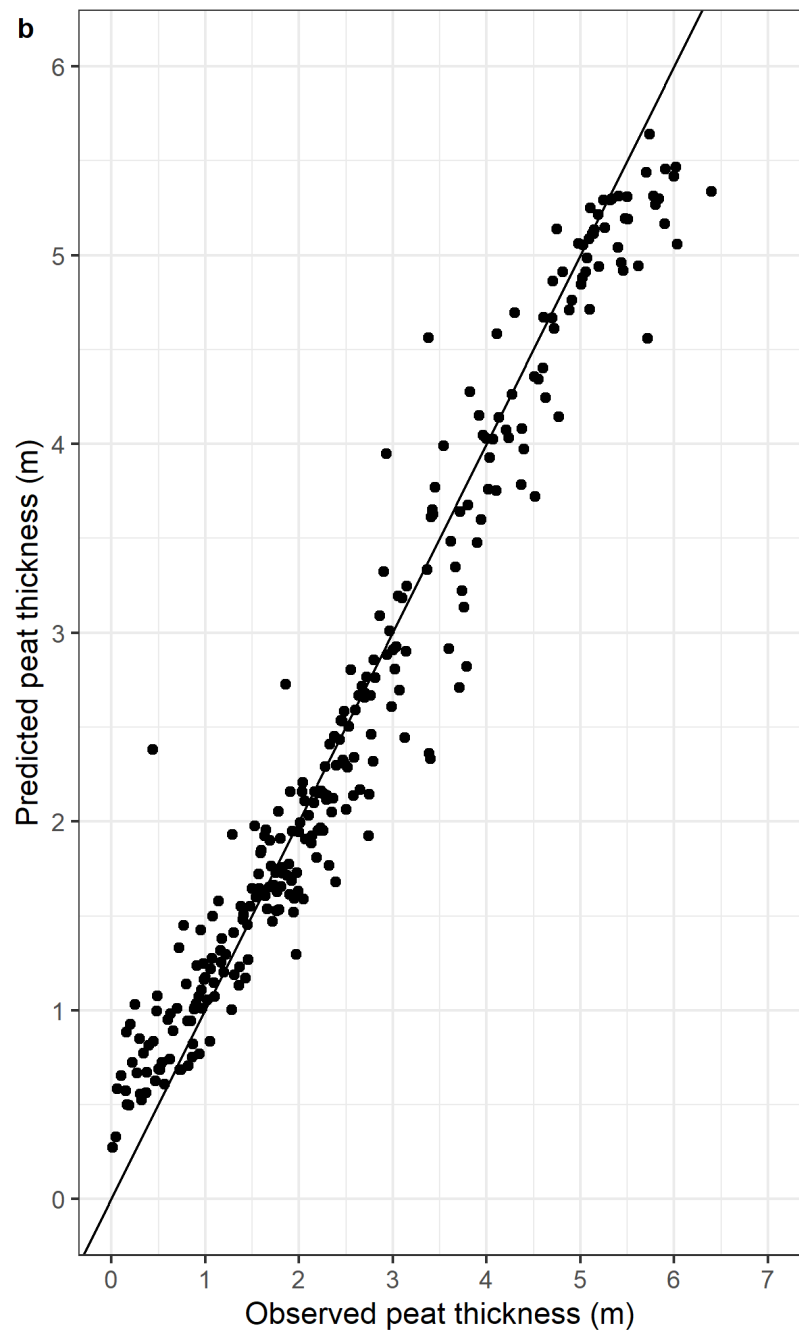
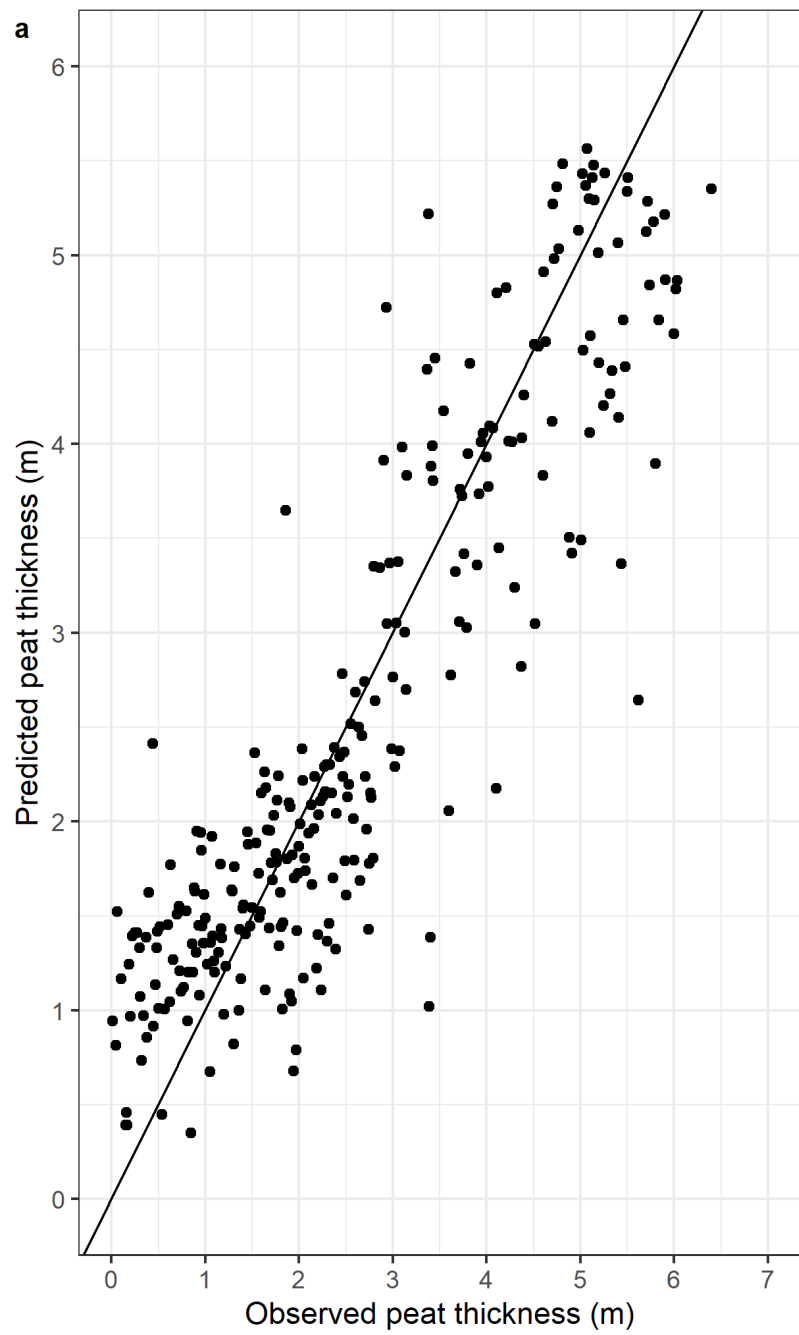
Country	Region	Peatland area (km ²)	Peat thickness (m)	Peat carbon density (Mg C ha ⁻¹)	Peat carbon stock (Pg C)
Republic of the Congo (ROC)	Likouala	28,636	1.9 ± 1.0	1,815 ± 740	5.4 (4.8 - 5.8)
	Cuvette	17,757	1.6 ± 0.8	1,626 ± 624	2.9 (2.7 - 3.2)
	Sangha	7,465	1.1 ± 0.4	1,218 ± 325	0.9 (0.8 - 1.0)
	Plateaux	1,183	0.9 ± 0.1	1,059 ± 162	0.1 (0.1 - 0.1)
	Total ROC	55,072	1.7 ± 0.9	1,653 ± 687	9.3 (8.4 - 10.2)
Democratic Republic of the Congo (DRC)	Équateur	58,276	1.9 ± 0.9	1,822 ± 658	10.7 (9.9 - 11.7)
	Mai-Ndombe	29,825	1.8 ± 0.7	1,752 ± 548	5.2 (4.8 - 5.7)
	Tshuapa	11,628	1.9 ± 0.5	1,917 ± 343	2.1 (1.8 - 2.6)
	Sud-Ubangi	7,557	1.1 ± 0.4	1,243 ± 370	1.0 (0.8 - 1.2)
	Mongala	5,329	1.2 ± 0.4	1,259 ± 360	0.6 (0.5 - 0.8)
	Total DRC	113,201	1.8 ± 0.8	1,740 ± 604	19.6 (17.9 - 21.9)
ROC and DRC combined	Total central Congo Basin peatlands	167,648 (159,378 - 175,079)	1.7 ± 0.9	1,712 ± 634	29.0 (26.3 - 32.2)

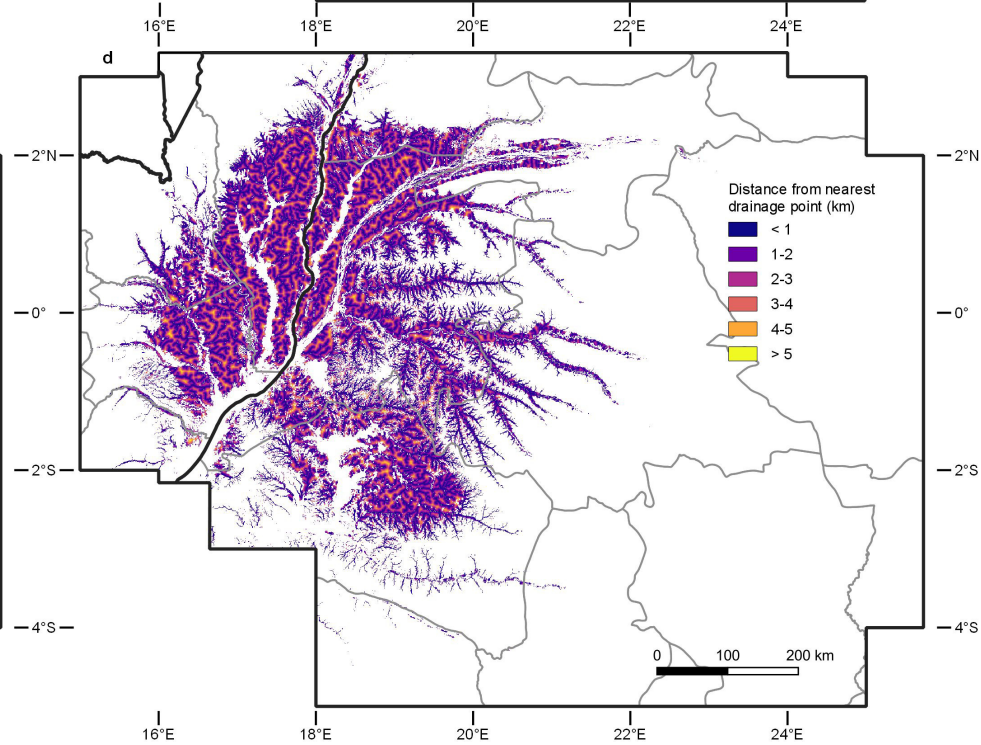
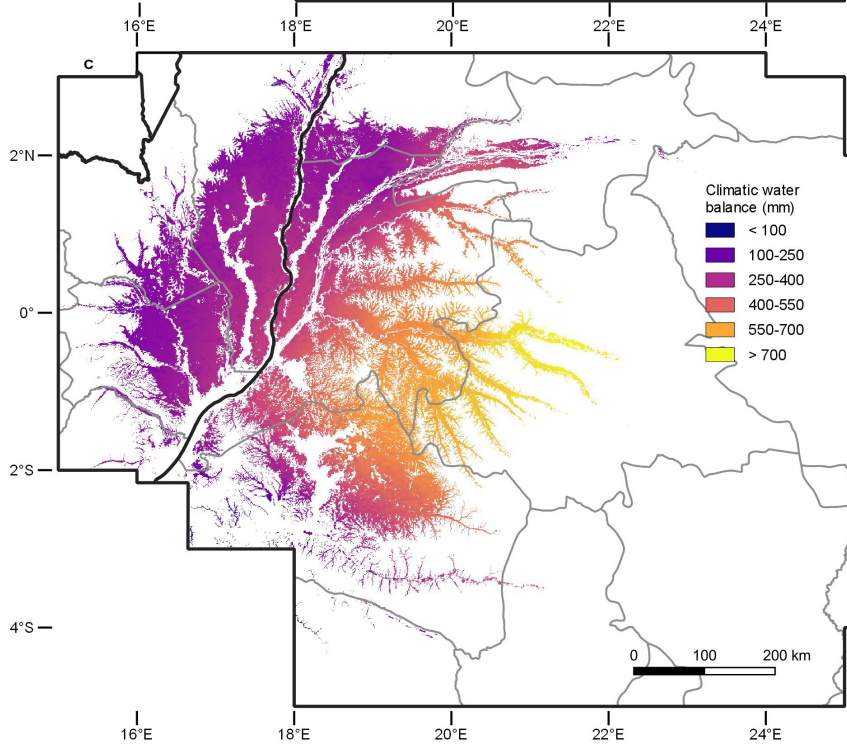
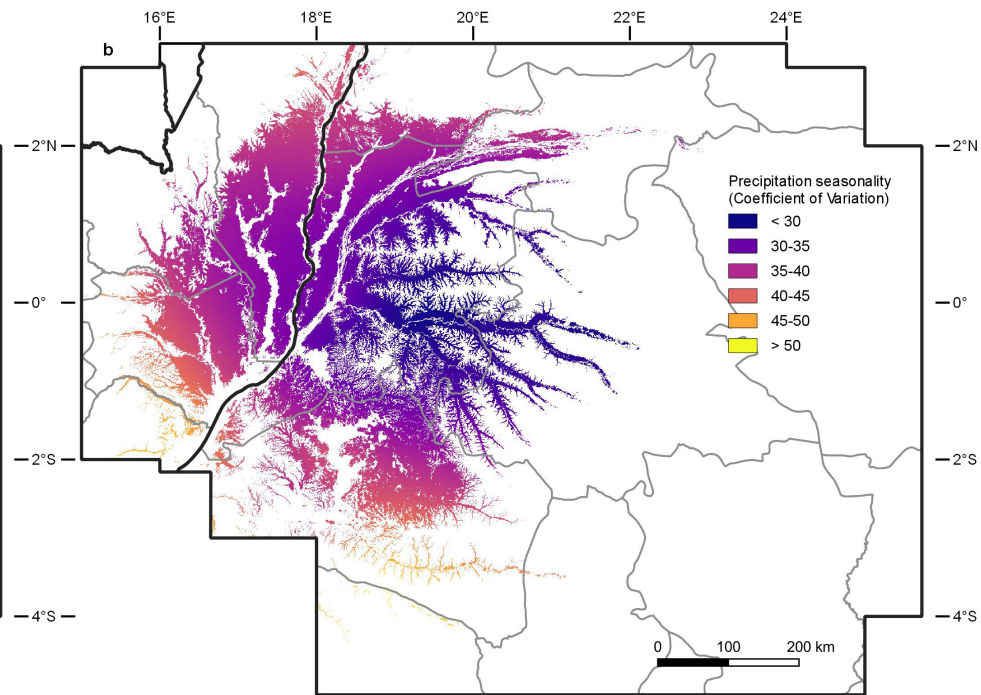
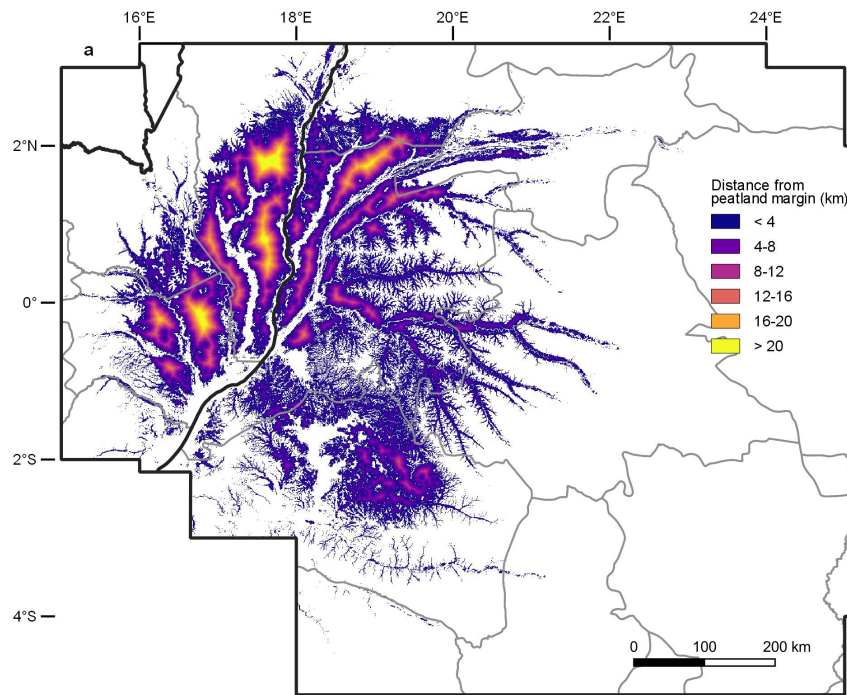


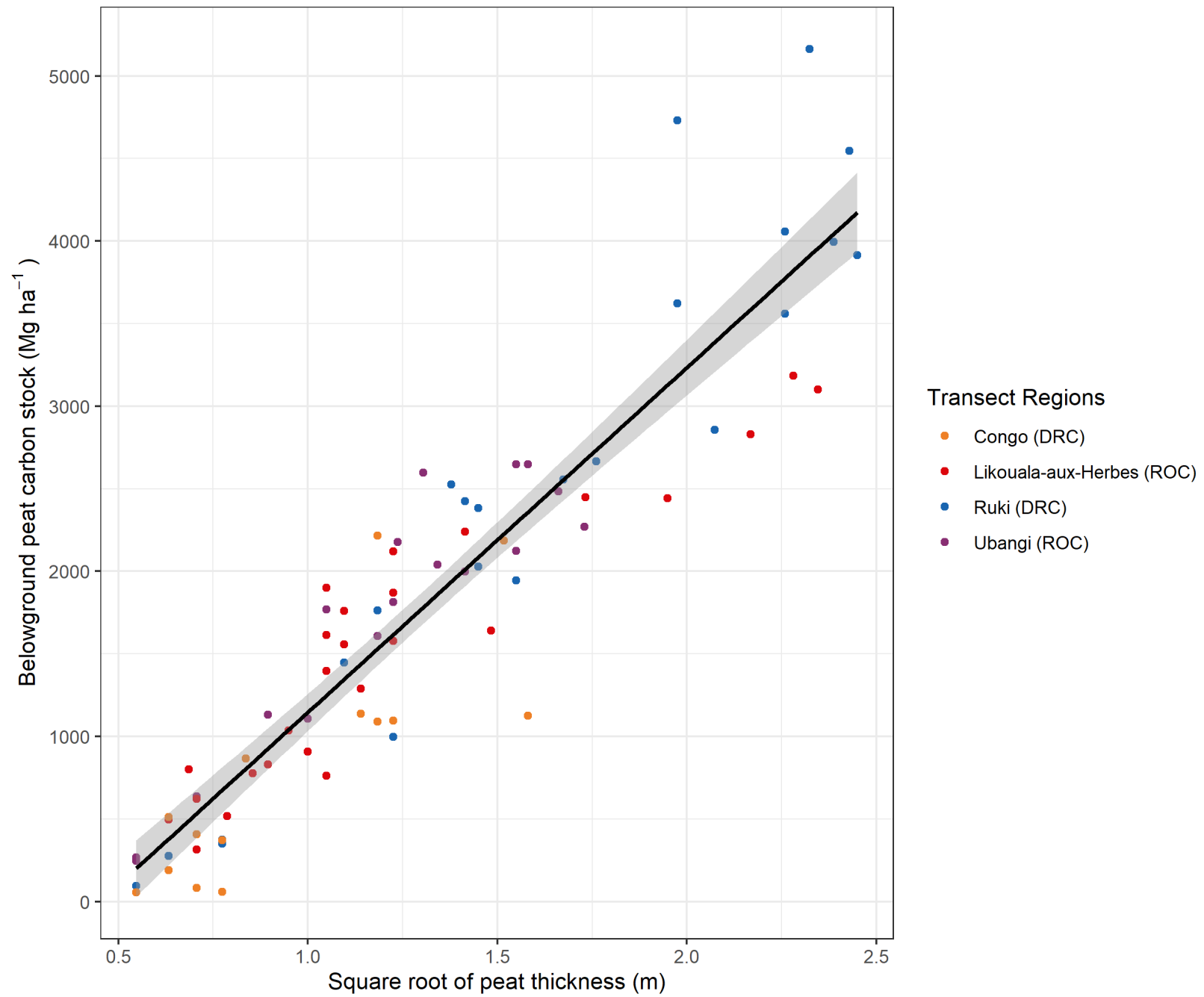
Transect Regions

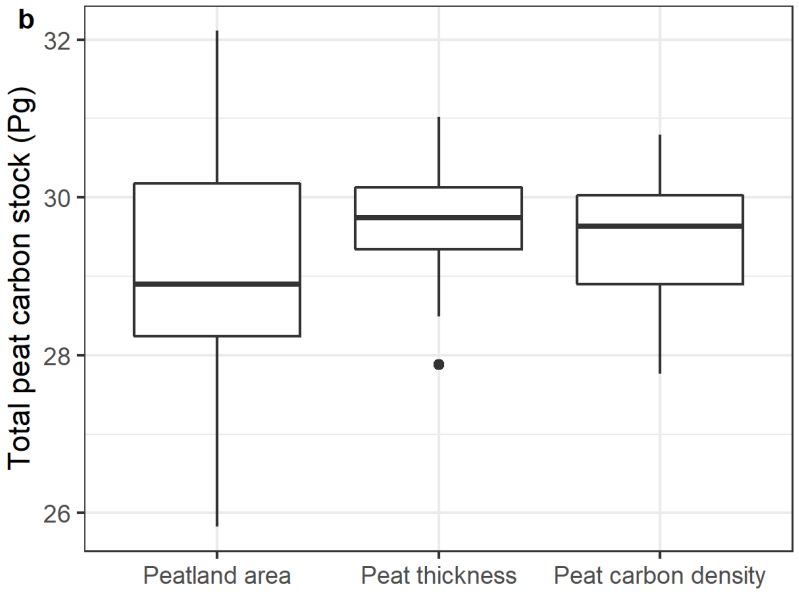
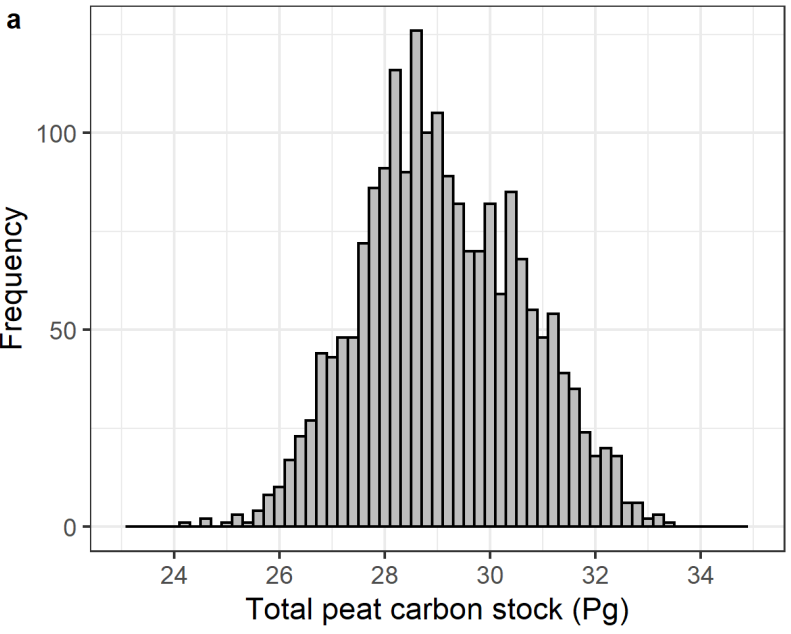
- Likouala-aux-Herbes + Ubangi (ROC)
- Congo + Ruki (DRC)

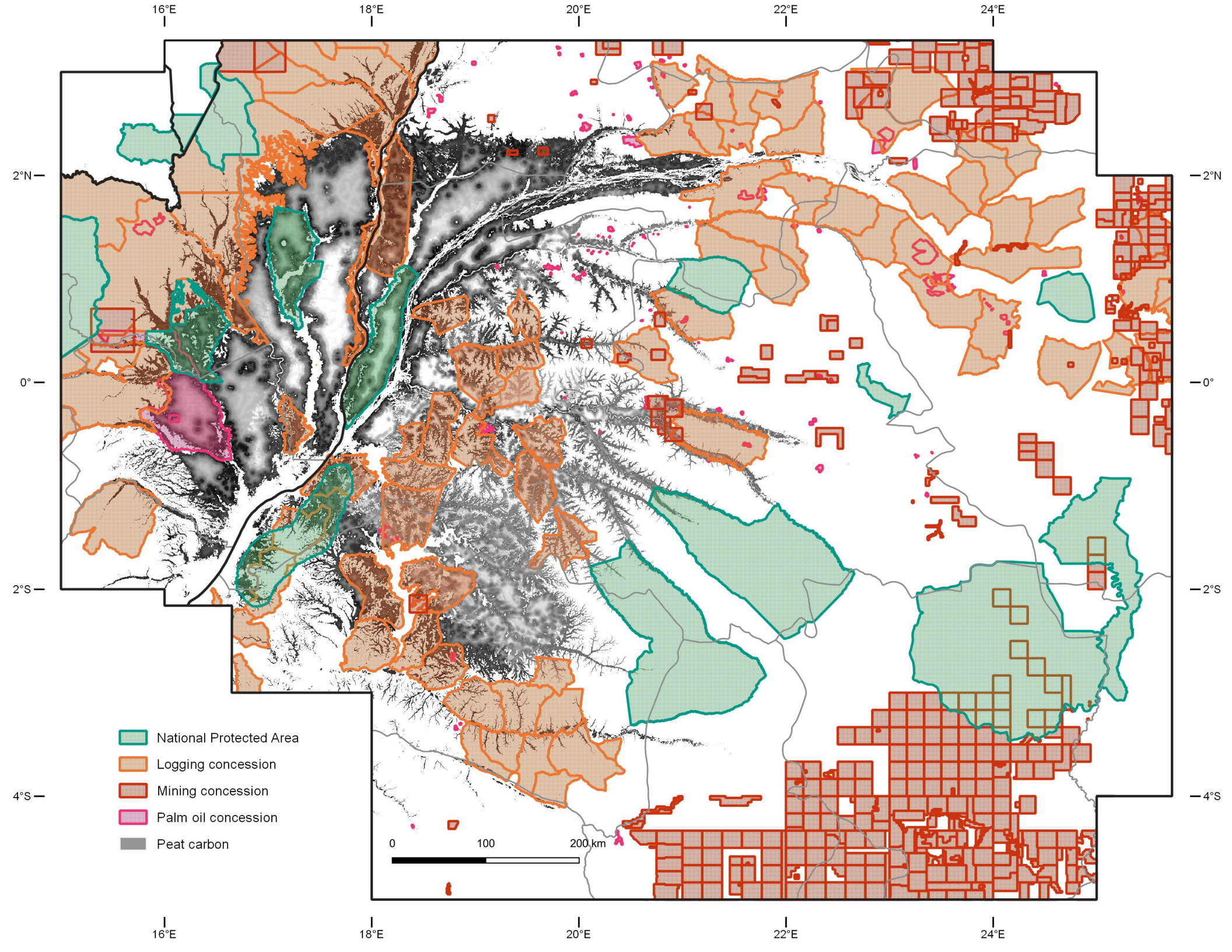












Country	Concessions / Protected areas	Peatland area (km²)	Peat thickness (m)	Peat carbon density (Mg C ha⁻¹)	Peat carbon stock (Pg C)
Republic of the Congo (ROC)	Industrial logging / mining / palm oil concessions	13,539 (25%)	1.2 ± 0.6	1,299 ± 451	2.0 (22%)
	National-level protected areas	6,402 (12%)	1.4 ± 0.6	1,463 ± 478	1.0 (11%)
Democratic Republic of the Congo (DRC)	Industrial logging / mining / palm oil concessions	29,712 (26%)	1.6 ± 0.7	1,671 ± 567	5.4 (28%)
	National-level protected areas	8,105 (7%)	1.5 ± 0.8	1,552 ± 592	1.4 (7%)
ROC and DRC combined	Industrial logging / mining / palm oil concessions	43,250 (26%)	1.5 ± 0.7	1,551 ± 560	7.4 (26%)
	National-level protected areas	14,511 (9%)	1.5 ± 0.7	1,513 ± 547	2.4 (8%)